Geochimica et Cosmochimica Acta, Vol. 69, No. 11, pp. 2829–2845, 2005
Copyright © 2005 Elsevier Ltd
Printed in the USA. All rights reserved
0016-7037/05 $30.00 + .00

doi:10.1016/j.gca.2005.01.012

Kimberlite petrogenesis: Insights from clinopyroxene-melt partitioning experiments at 6 GPa in the CaO-MgO-Al_2O_3-SiO_2-CO_2 system

Shantanu Keshav,[1,2,*] Alexandre Corgne,[1] Gudmundur H. Gudfinnsson,[1] Michael Bizimis,[3] William F. McDonough[4] and Yingwei Fei[1]

[1]Geophysical Laboratory, Carnegie Institution of Washington, Washington DC 20015, USA
[2]Department of Geological Sciences, Case Western Reserve University, Cleveland, OH 44106, USA
[3]National High Magnetic Field Laboratory, Isotope Geochemistry, and Department of Geological Sciences, Florida State University, 1800 E. Paul Dirac Drive, Tallahassee, FL 32306, USA
[4]Department of Geology, University of Maryland, College Park, MD 20742, USA

(*Received August* 16, 2004; *accepted in revised form January* 18, 2005)

Abstract—In this experimental study, we examine the mineral-melt partitioning of major and trace elements between clinopyroxene and CO_2-rich kimberlitic melts at a pressure of 6 GPa and temperatures of 1410°C and 1430°C. The melts produced contain ~ 28 wt% dissolved CO_2, and are saturated with olivine and clinopyroxene. To assess the effects of temperature, crystal and melt compositions on trace element partitioning, experiments were performed in the model CaO-MgO-Al_2O_3-SiO_2-CO_2 system. Our results reveal that all the elements studied, except Al, Mg, Si, and Ga, are incompatible in clinopyroxene. Partition coefficients show a considerable range in magnitude, from ~ 10^{-3} for D_U and D_{Ba} to ~ 2.5 for D_{Si}. The two experimental runs show similar overall partitioning patterns with the D values being lower at 1430°C. Rare earth elements display a wide range of partition coefficients, D_{La} (0.012–0.026) being approximately one order of magnitude lower than D_{Lu} (0.18–0.23). Partition coefficients for the 2+ and 3+ cations entering the M2-site exhibit a near-parabolic dependence on radius of the incorporated cations as predicted from the lattice strain model. This underlines the contribution made by the crystal structure toward controlling the distribution of trace elements. Using data obtained in this study combined with that in the published literature, we also discuss the effects that other important parameters, namely, melt composition, pressure, and temperature, could have on partitioning.

Our partition coefficients have been used to model the generation of the Group I (GI) kimberlites from South Africa. The numerical modeling shows that kimberlitic melts can be produced by ~0.5% melting of a MORB-type depleted source that has been enriched by small-degree melts originating from a similar depleted source. This result suggests that the source of GI kimberlites may be located at the lithosphere-asthenosphere transition. Percolation of small degree melts from the asthenosphere would essentially create a metasomatic horizon near the bottom of the non-convecting sublithospheric mantle. Accumulation of such small degree melts together with the presence of volatiles and conductive heating would trigger melting of the ambient mantle and subsequently lead to eruption of kimberlitic melts. Additionally, our model shows that the GI source can be generated by metasomatism of a 2 Ga old MORB source ca. 1 Ga ago. Assuming that MORB-type mantle is the most depleted source of magmas on earth, then this is the oldest age at which the GI source could have existed. However, this age most likely reflects the average age of a series of metasomatic events than that of a single event. *Copyright © 2005 Elsevier Ltd*

1. INTRODUCTION

Their widespread geographical distribution, deep origin, unique geochemistry, and age span from late Precambrian to the Cretaceous make kimberlites particularly appropriate for investigating the chemical evolution of the Earth's upper mantle (Bell and Blenkinsop, 1987). Kimberlites, like carbonatites, are rare, but have been found on almost every continent, and are also the principal transporter of a variety of xenoliths from crustal and mantle depths. Importantly, these mantle xenoliths brought up by kimberlites are the primary source of information on the nature of physico-chemical processes in the mantle, and even more so, the continental mantle (Pearson et al., 2004). Kimberlites form part of a spectrum of silica-undersaturated rocks that vary widely in composition and include such rock types as melilitites, lamprophyres, and nephelinites. The petrogenesis of kimberlites is, however, controversial, with disagreements over the nature and depth of the source region, whether they are primary in origin, and the cause of melting (e.g., plume vs. volatile fluxing).

On the basis of thermobarometry on xenoliths brought up by the kimberlites, the mantle parentage of these rocks is without doubt and attention has focused on the role of CO_2 in melting of peridotite under upper-mantle conditions (Canil and Scarfe, 1990; Dalton and Presnall, 1998b; Gudfinnsson and Presnall, 2003,, in press). From such experimental studies, it is now well established that initial melts from carbonated lherzolite at pressures in excess of ~ 3 GPa are CO_2-rich (> 40 wt%) and SiO_2-poor (< 10 wt%), and are thus carbonatitic in character (Green and Wallace, 1988; Wallace and Green, 1988; Thibault et al., 1992; Dalton and Wood, 1993; Dalton and Presnall, 1998a; Gudfinnsson and Presnall, 2003, in press). Some kimberlite magmas are derived by melting of the asthenospheric mantle, as indicated by the geochemistry (Smith et al., 1985).

* Author to whom correspondence should be addressed (s.keshav@gl.ciw.edu).

Due to the high concentrations of incompatible trace elements measured in kimberlites and carbonatites, generation by very small degree of melting has been inferred (Nelson et al., 1988; Bizimis, 2001; le Roex et al., 2003). However, apart from the earlier work of Canil and Scarfe (1990), it is only recently that phase equilibrium studies pertaining to the generation of kimberlites at high pressures, corresponding to the diamond stability field, have become available (Dalton and Presnall, 1998a, 1998b; Gudfinnsson and Presnall, 2003, in press), where some kimberlite magmas must originate.

CO_2-rich melts are also frequently invoked as agents of metasomatic mass transfer in the upper mantle (Green and Wallace, 1988; Yaxley et al., 1991; Hauri et al., 1993; Rudnick et al., 1993; Yaxley et al., 1998). Combined with their extreme mobility (Hunter and McKenzie, 1989; Minarik and Watson, 1995) this makes CO_2-rich melts (kimberlites and carbonatites) very efficient metasomatising agents. However, only rarely do metasomatised mantle rocks themselves preserve unambiguous evidence for the passage of CO_2-rich melts, such as carbonate crystals (Ionov et al., 1993, 1996; Yaxley et al., 1998). In no case is the pristine agent affecting the ambient mantle itself preserved, and thus its composition must always be inferred through calculation (Hauri et al., 1993; Rudnick et al., 1993). However, such calculations hinge critically on assumptions about the partitioning of trace elements between mantle minerals (such as clinopyroxene/garnet) and CO_2-rich melts, for which there are few experimental data. Consequently, while trace element partitioning between clinopyroxene (cpx) and basaltic (mainly tholeiitic) liquids is increasingly well understood (e.g., Wood and Blundy, 1997; Blundy et al., 1998; Johnson, 1998; Salters and Longhi, 1999; Hill et al., 2000; Salters et al., 2002; McDade et al., 2003), there is no consensus on whether partitioning between cpx and CO_2-rich melts is broadly similar (Brenan and Watson, 1991), or whether it shows significant quantitative differences for some elements (Green et al., 1992; Walker et al., 1992; Jones et al., 1995; Klemme et al., 1995; Blundy and Dalton, 2000). If the latter is true, then it may be possible to identify chemical fingerprints that allow carbonate melt metasomatism to be distinguished from that due to silicate or hydrous melts. In addition, in the absence of a set of appropriate partition coefficients that are suitable to model mantle melting processes, either the available data on basaltic liquids or an average of mineral-CO_2-rich melt partition coefficients from published literature are used. Thus, in this contribution, we present the results of major- and trace element partitioning experiments between clinopyroxene and CO_2-rich melts at 6 GPa and temperatures of 1410 and 1430°C. To our knowledge, these are the first high-pressure partitioning results between a mantle phase and kimberlitic melt, and thus are of direct relevance toward understanding the petrogenesis of these low-degree, highly potent, and very low viscosity CO_2-rich melts. Pressure of 6 GPa, approximating the pressure at a depth of $\sim$ 200 km, was chosen because it closely corresponds to the pressure at the top of the asthenosphere beneath cratons on most of the continents (for example, South Africa and Siberia; Pearson et al., 2004), and also because there is geochemical evidence suggesting the generation of at least some kimberlite magmas deep in the asthenosphere. We note, however, that models invoking the generation of kimberlites at both shallower and deeper mantle levels have also been proposed (Haggerty, 1994; Bizimis, 2001; le Roex et al., 2003).

Partitioning of a trace element between cpx and kimberlitic melt is likely a complex function of pressure (P), temperature (T), and phase composition, and it is unlikely that a single set of partition coefficients will suffice under all conditions relevant to the generation of these melts in the Earth's mantle. Nonetheless, most of the high P-T experiments relevant to mantle melting in the past, that have dealt with trace element partitioning between mantle phase(s) and CO_2-rich melts, have used natural starting compositions, and have applied their results to the petrogenesis of carbonatites and also in a few cases, kimberlites (Green et al., 1992; Klemme et al., 1995; Adam and Green, 2001). Unfortunately, this approach rarely yields unique results. For example, in the case of mantle melting at the solidus of anhydrous mantle lherzolite, some studies (Blundy et al., 1998; Salters and Longhi, 1999; Salters et al., 2002) have produced quite conflicting results. Without an understanding of the controls on element partitioning, these conflicts cannot be accounted for, and the users of these partitioning datasets are left unsure which set best describes the mantle melting process. Unless experiments are designed to reduce the number of influential parameters, it is difficult to assess whether differences in partitioning behavior are due solely to differences in melt chemistry and melt structure (Gaetani, 2004), or whether they are a consequence of differences in P, T, and crystal composition (Gaetani and Grove, 1995; Blundy et al., 1998; Lundstrom et al., 1998; Salters and Longhi, 1999; Salters et al., 2002). Thus, the present sets of experiments were conducted in the system CaO-MgO-Al_2O_3-SiO_2-CO_2 (CMAS-CO_2), with the intention of assessing the individual contributions of phase composition and temperature to the partitioning process. We exploit the opportunity to compare trace element partitioning in the presence of two compositionally distinct kinds of cpx coexisting with kimberlitic melts at 6 GPa and 1410 and 1430°C.

In this contribution we wish to address the following: (1) Is the cpx-melt partitioning of trace elements different for basaltic, carbonatitic, and kimberlitic melts? (2) At a fixed pressure, what is the effect of temperature and phase composition on trace element partitioning? (3) Using the partition coefficients obtained in this study, can we constrain the origin of kimberlitic melts in the Earth's mantle?

2. PHASE EQUILIBRIA IN THE CaO-MgO-Al_2O_3-SiO_2-CO_2 SYSTEM

As we have chosen to use the model system CMAS-CO_2 to explore the behavior of trace element partitioning, a brief discussion of phase equilibrium systematics is warranted. In the system CMAS-CO_2, kimberlitic melts coexist with a four-phase garnet lherzolite mantle assemblage along a divariant surface in P-T space (Dalton and Presnall, 1998a, 1998b; Gudfinnsson and Presnall, 2003, in press; Fig. 1). At a fixed P and T, the garnet lherzolite plus liquid (kimberlitic) assemblage is invariant, and compositions of all the phases, independent of the bulk composition, are uniquely defined. On the high-temperature side, the divariant surface is bounded by the CO_2-free garnet lherzolite solidus (Fig. 1), whereas on the low-temperature side, the surface is bounded by the univariant solidus

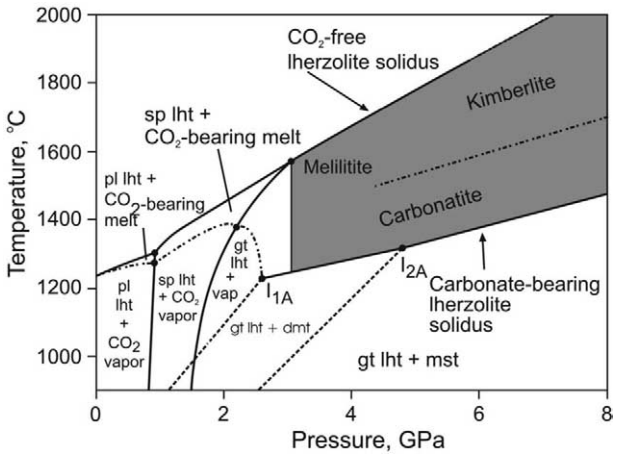

Fig. 1. Pressure-temperature diagram for the solidus of plagioclase, spinel, and garnet lherzolite in the CMAS system under CO_2-free and CO_2-bearing conditions. This diagram has been modified after Dalton and Presnall (1998a) and Gudfinnsson and Presnall (2003, in press). The divariant region between the CO_2-bearing (carbonate-bearing above 2.6 GPa) and CO_2-free solidi is divided into three different areas; an area where CO_2-bearing melt coexists with (1) plagioclase lherzolite phase assemblage; (2) spinel lherzolite phase assemblage, and (3) garnet lherzolite phase assemblage. The points on the CO_2-bearing solidus curve at ~2.8 and 4.8 GPa (marked I_{1A} and I_{A2}; Dalton and Presnall, 1998a) denote the transitions on the solidus from CO_2 vapor-bearing to dolomite-bearing garnet lherzolite and dolomite-bearing to magnesite-bearing garnet lherzolite, respectively. The subsolidus univariant lines originating from these points are also shown. The intersection of the spinel- to garnet lherzolite transition with the subsolidus univariant line extending from the invariant point I_{1A} is uncertain (Gudfinnsson and Presnall, 2003, in press). The dashed line on the divariant surface indicates the approximate division in the system between carbonatitic melts, on the one hand, and kimberlitic and melilititic melts, on the other. Gt, garnet; dmt, dolomite; mst, magnesite; pl, plagioclase; sp, spinel; vap, CO_2 vapor; lht, lherzolite.

curve along which the garnet lherzolite phase assemblage is joined by either dolomite, magnesite, or CO_2 vapor (Fig. 1). At a given pressure, the solidus of model carbonated lherzolite in the system CMAS-CO_2 corresponds to an invariant point on this latter univariant curve where olivine + orthopyroxene + clinopyroxene + garnet + carbonate + liquid coexist. By determining the compositions of all the phases at this point, it is possible, through the algebraic methods described by Presnall (1986), to determine whether the point is a eutectic or peritectic. This technique cannot be rigorously applied to natural, multi-component systems because of their high variance.

One of the main advantages in using the CMAS-CO_2 system is that the starting compositions can be constructed such as to maximize the amount of liquid in the run products, and the resulting phase equilibrium data can be used to model very small degree melting in the mantle. Thus, in the CMAS-CO_2 system, melts analogous to very small degree natural melts can readily be analyzed using the electron microprobe. In natural systems, in contrast, it is hard to maintain equilibrium during experiments because of the small amount of melt present, and the melts generated are invariably modified upon quenching and impossible to analyze because of their very small volume. Hence, by reducing the number of components, and by implication the variance of the system, the task becomes easier to handle, and quantitative information on phase equilibria and the partitioning behavior can be determined rigorously. Components other than CaO, MgO, Al_2O_3, SiO_2, and CO_2 are all, except FeO and H_2O, in such a low abundance that their effects on the phase equilibria are likely to be minor (Gudfinnsson and Presnall, 2003, in press). The effects of FeO and Na_2O on the stability of carbonates, and by implication, the carbonate-bearing solidus, are more uncertain, however.

3. EXPERIMENTAL AND ANALYTICAL PROCEDURES

The major-element composition used in this study is the JADSCM-3 used in previous phase equilibrium studies (Dalton and Presnall, 1998a, 1998b; Gudfinnsson and Presnall, 2003, in press). The JADSCM-3 composition (in wt%) is as follows: CaO—21.36; MgO—25.68; Al_2O_3—3.04; SiO_2—27.54; CO_2—22.82. One gram of JADSCM-3 was prepared from high purity oxides and carbonates ($CaCO_3$). Carbon dioxide was added as natural magnesite (Victoria, Australia), kindly donated by Dr. David Green, which contains <0.5 wt% $CaCO_3$ and <0.03 wt% $FeCO_3$ (Brey et al., 1983). The high-purity oxides were fired in high-temperature furnaces in Pt-crucibles in the following manner: MgO at 1250°C for 24 hours; Al_2O_3 at 1200°C for 12 hours, and SiO_2 at 1200°C for 6 hours. The oxides (after firing) and $CaCO_3$ (the source of CaO) were stored under vacuum before mixing them in appropriate proportions. The silicate portion of the starting material was ground for one hour in an agate mortar under ethanol to a fine homogeneous powder. After drying, this oxide and carbonate mixture was decarbonated in air in a box furnace. The decarbonation temperature of calcite, at 1 atmospheric pressure is 898°C, and the following steps were undertaken to decarbonate the silicate portion of the starting material: (1) The mixture was poured into a Pt-crucible with the lid on top, and kept in the furnace; (2) Temperature of the furnace was initially raised to 600°C, and then gradually to 1000°C over a period of ~ 2 hours; (3) The Pt-crucible was kept at 1000°C for 20 min. After this step, the Pt-crucible was taken out of the furnace, was cooled in air for ~ 15 min, contents of the crucible carefully poured in a vial, and stored under vacuum. To ensure homogeneity, the silicate portion of JADSCM-3 was finely re-ground as before, then dried, and finally fused for 4 hours at 1550°C in a Pt-crucible and quenched. The resulting glass (optically transparent) was ground for one hour to a fine powder under ethanol in an agate mortar.

As most of the MgO and all of the CO_2 in JADSCM-3 are provided by magnesite, to prevent decarbonation of magnesite, it was necessary to dope the silicate portion of JADSCM-3 before mixing magnesite into it. This glass mixture (1 g) was doped with a suite of trace elements (Rb, Sr, Ba, Pb, Yb, Lu, Sm, Nd, Y, Ga, La, Sc, Ce, U, Th, Hf, Zr, Ti, Nb, and Ta) at levels between 50 and 500 ppm, using 1000 μg/g AAS standard solutions in nitric acid. After the first few doping sessions, the mixture was ground in an agate mortar, and dried under a heat lamp for ~10 min. The rest of the elements were then added, and the doped mixture dried as before. This mixture was denitrified in air at 400°C for four hours in a Pt-crucible. After denitrification, the doped powder was stored under vacuum.

Magnesite, the source of MgO and CO_2 in JADSCM-3 was ground under ethanol in an agate mortar for 1 h, and was dried for 14 hours at 250°C in a Pt-crucible. The doped silicate

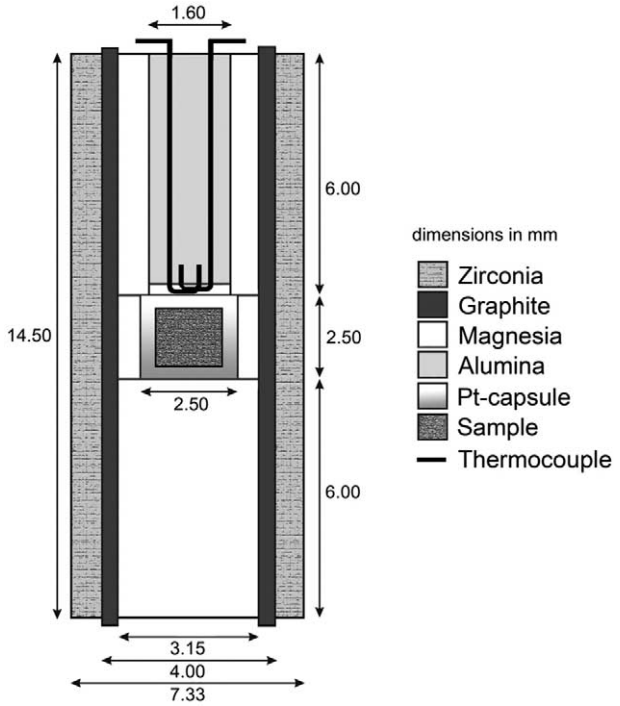

Fig. 2. Cross section of the 18 mm pressure cell used in the present study.

portion of JADSCM-3 was added to magnesite in an agate mortar. To ensure homogeneity, the mixture was ground for more than an hour, and stored under vacuum.

~1.2–1.5 mg of the doped starting material was loaded into a 1.2 mm outer diameter platinum capsule that had previously been annealed (600°C), boiled in dilute HCl (10 min), and sealed at one end by arc welding. The capsule plus the starting material was dried at 250°C for at least 12 hours, weighed, welded shut, and weighed again. Following the procedures outlined by Dalton and Presnall (1998a, 1998b), capsules were discarded if a weight loss of >10 wt% (excluding the capsule weight) due to decarbonation occurred during the final welding. After welding both the ends, the final capsule length was 2 mm.

All the high-pressure, high-temperature partitioning experiments were conducted using a split-cylinder multi-anvil device (MA6/8; Presnall-type) at the Geophysical Laboratory. The experiments reported here were performed at 6 GPa using MgO cast octahedra with fins (Ceramacast; Aremco Products Inc, NY, USA) with an effective edge length of 18 mm as pressure cells. The furnace assembly (Fig. 2) in this type of cell consists of a thick zirconia sleeve (acting as the thermal insulator) surrounding a straight graphite furnace with inner MgO spacers, and 4-hole alumina thermocouple sleeve. Tungsten-carbide (WC), second-stage anvils with 11 mm truncated edge lengths (TEL) were used to impart pressure on the cell. Pressure calibrations were done at 1200°C as described by Walter et al. (1995), and the precision in pressure is estimated to be ± 0.2 GPa. To ensure near-anhydrous run conditions, the octahedra, zirconia and MgO sleeves, and the end-plugs were fired just before the experiments at 1000°C for 1 h. After construction, the entire cell was kept at 110°C.

Temperatures were measured using Type-C (W26Re-W5Re) thermocouples with no correction for the effect of pressure on the thermocouple *emf*, and were controlled automatically to within ± 3°C. The thermocouples were positioned along the axis of the graphite furnace, and in contact with the Pt-capsules, which were encased in MgO sleeves ~ 2.2–2.5 mm in length (Fig. 2). The temperature gradient across the Pt-capsule in this set of experiments is believed to be within ± 20 to 25 °C. This estimation is based on the results from Walter et al. (1995) and van Westrenen et al. (2003) at similar *P-T* conditions for a cell design with a straight graphite heater similar to the one used in this study. Dalton and Presnall (1998a, 1998b) and Gudfinnsson and Presnall (2003, in press) used a cell design also similar to ours, with an identical Pt-capsule length (2 mm before compression) but with a stepped graphite furnace, for which a thermal gradient of ± 15°C was reported. The results of Walter et al. (1995) and van Westrenen et al. (2003) and the fact that identical phase relations were obtained with our cell design (experiments not reported here) and the one used in the studies of Presnall and coworkers indicate that the use of a straight graphite furnace increases the temperature gradient only slightly across the capsule, on the order of 5 to 10 °C. Assemblies were pressurised at 0.75 GPa/h to the desired pressure of 6 GPa. Temperature was raised at 100°C per minute. To grow large crystals, the temperature was raised to at least 60°C above that of the final target temperature, and then lowered to the target temperature at 1°C/min. Due to the degradation of the graphite furnace, the total run duration (besides the cycling time) at the target temperature was limited to 6 hours for the experiments reported here. The experiments were automatically quenched, with a quench rate of 500°C/s. During the entire run duration, both power and temperature were extremely stable. The runs were decompressed over a course of 5–6 hours. The run conditions along with the phase assemblage in these experiments are shown in Table 1.

Table 1. Experimental conditions and results.

Run No.	*P* (GPa)	*T* (°C)	*t* (h)	Assemblage[x]
PR-168	6.0	1430	6	qnch (85) + cpx (12) + ol (3)[a]
PR-170	6.0	1410	6	qnch (83) + cpx (10) + ol (7)

[x] Abbreviations are as follows: qnch — quenched melt; cpx — clinopyroxene; ol — olivine; *P* — pressure; *T* — temperature; *t* — run duration in hours (h)

[a] numbers in parentheses represent approximate mode (wt.%) of the run products

The recovered capsules were mounted in Petropoxy-154 resin and polished longitudinally for optical and chemical analyses. Due to the high solubility of the carbonate-rich melt in water, the run products were polished in oil using SiC grit (240–600) paper. Additionally, because of the highly fragile nature of the charge, it was necessary to vacuum-impregnate the run products at least twice with Petropoxy-154 resin and regrind until a satisfactory surface for diamond polishing (3–0.25 μm) was obtained.

Major element compositions of the quenched melt were obtained using a JEOL JXA 8800 electron microprobe at the Geophysical Laboratory, with an accelerating voltage of 15 kV, a rastering beam of 20–120 μm^2, and a 15 nA probe current (at

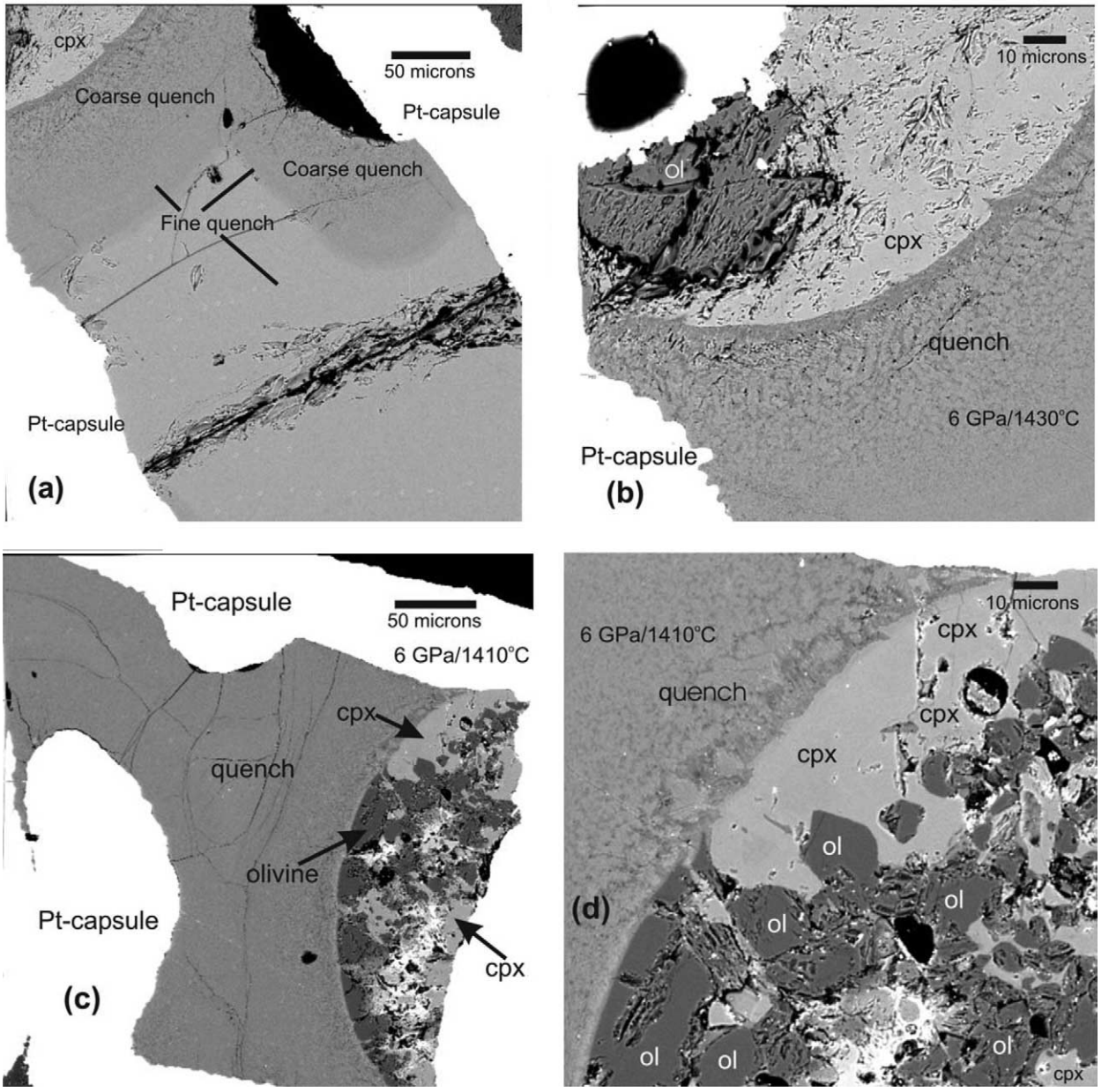

Fig. 3. Back-scattered electron images of the experimental run products in this study (a) a nearly complete section of the platinum capsule for the run PR168. To be noted is the gradation from relatively fine to coarse quench near the crystalline solids portion. The hemisphere at the top corner is a vesicle originally filled with CO_2; (b) a close-up of PR168 showing in detail the texture of the run products; (c) sectioned platinum capsule of the run PR170 showing segregation of the crystalline and quench products; (d) a close-up of PR170. Note the olivine inclusions (dark) in relatively lighter clinopyroxene. In all the pictures, the abbreviations are as follows: ol, olivine; cpx, clinopyroxene.

the Faraday cup). The melt is composed of a very fine textured intergrowth of Ca-Mg carbonates and quench silicate phases (Fig. 3). Thus, representative analyses cannot be obtained with the analytical procedure used for silicates because carbon is missing from the correction routine. Analyses were reduced using the ZAF correction routine and the amount of CO_2 in the melt regions was calculated by difference. In calculating the matrix corrections for melts, the program assumes that the oxide not being analyzed is CO_2. This is not an ideal procedure, but is currently the most satisfactory available. Crystalline phases were analyzed using 1 μm spot mode. The major element compositions of the run products are shown in Table 2. At least 30 and 65 analyses of the crystalline solids and melt, respectively, were acquired.

Trace elements were determined using the laser ablation inductively coupled plasma mass spectrometry (LA-ICP-MS) facility at Department of Geology at the University of Maryland. This laser system employs a frequency-quintupled Nd:YAG laser operating at 213 nm (UP213 from New Wave Research), coupled to an Element 2 (Thermo Finnigan MAT)

Table 2. Major element compositions (wt.%) of the run products in the present set of experiments. Two standard errors in terms of least units cited (in parentheses) of *n* (no. of analyses) EPMA analyses also provided.

Run No.	PR-168	PR-170
P (GPa)	6	6
T (°C)	1430	1410
Quench		
n	59	60
SiO_2	22.08 (4)	21.60 (17)
Al_2O_3	3.07 (1)	3.60 (4)
MgO	23.95 (3)	20.43 (16)
CaO	22.88 (2)	27.15 (9)
CO_2[a]	28.00	27.21
Sum[b]	71.99 (2)	72.79 (12)
Ca/Ca + Mg	0.49	0.57
Mg/Ca	1.04	0.75
Mode (wt.%)	85	83
Olivine		
n	35	28
SiO_2	43.60 (24)	43.59 (28)
Al_2O_3	0.05 (2)	0.04 (1)
MgO	56.50 (32)	56.60 (33)
CaO	0.14 (4)	0.12 (3)
Sum	100.29 (15)	100.35 (16)
Mode (wt.%)	3	7
Cpx		
n	31	35
SiO2	55.37 (13)	53.23 (17)
Al_2O_3	3.55 (19)	4.96 (20)
MgO	26.03 (22)	20.43 (19)
CaO	15.09 (23)	21.40 (14)
Sum	100.04 (19)	100.02 (17)
Mode (wt.%)	12	10
Cations per 6 oxygens in cpx		
Si	1.931	1.894
Al^{IV} (T)	0.068	0.105
Al^{VI} (M1)	0.077	0.102
Mg (M1)	0.918	0.900
Mg (M2)	0.436	0.184
Ca	0.564	0.815
Sum	3.993	3.999
CaTs[c]	0.082	0.100

[a] CO_2 calculated by difference.
[b] Sum without adding CO_2 in the quench.
[c] CaTs — Calcium-Tschermaks component in cpx

magnetic sector ICP-MS. The ablation cell was flushed with He to enhance sensitivity. Depending on the crystal size, laser parameters ranged from ~ 8–20 μm diameter, with 5–12 Hz frequency. A typical time-resolved analysis involved ~ 20 s of background acquisition with the ablation cell being flushed with He, followed by laser ablation for ~ 40 s. NIST 610 and BCR-2g (Columbia River Basalt-USGS reference glass standard) were used as primary calibration and secondary check standards, respectively. With the setup described above, the precision for the LA-ICP-MS technique is better than 15% on all measured masses. Contamination of the cpx analyses by neighboring phases is a major concern when measuring trace element contents of highly incompatible elements (e.g., Ba, U, Th). Although we took great care in selecting spectra (or part of spectra, when crystal thickness was less than the ablation pit) showing no sign of contamination (i.e., with constant count rate), cpx analyses may have suffered from a small amount (< 1%) of contamination by interstitial melt or olivine. Selected time-resolved spectra were processed off-line using a spreadsheet program to apply the background subtraction and calculation of absolute trace element abundances (modified version of LAMTRACE by Simon E. Jackson). Variations in ablation yields were corrected by reference to Ca concentrations measured by electron microprobe. Minimum detection limits for reported concentrations are calculated on the basis of 2σ above the background count rate.

4. ATTAINMENT OF EQUILIBRIUM AND WATER IN THE EXPERIMENTS

The experiments reported here were not reversed, and one must therefore look to other criteria to determine if the experiments approached equilibrium. Irving and Wyllie (1975) observed that the reaction rates in carbonate systems at high pressure and temperatures are quite rapid with equilibrium being attained in run times of less than 1 h. In slightly more complex carbonate-silicate systems, equilibrium has been demonstrated in run times of less than 5 hours on the basis of reversed reactions (Lee et al., 1994). Durations of our experiments were in excess of these values and the high proportion of liquid in our runs is likely to facilitate equilibrium. In fact, the elevated calcium content of olivines (Table 2) is consistent with equilibration with a Ca-rich liquid as has been previously noted (Dalton and Presnall, 1998b; Gudfinnsson and Presnall, 2003, in press). Detailed backscattered electron imaging of the run products did not reveal any zonation in the crystalline solids. Furthermore, electron probe profile analyses revealed no sign of major element zoning in both melt and cpx. Also, LA-ICPMS profile across large melt pockets provided similar trace element concentrations. However, because of the small crystal size compared to the LA-ICP-MS beam size, 'horizontal' trace element profiling across a single crystal was not possible. On the other hand, because the LA-ICP-MS technique allows data to be time resolved at a very small scale, information about the nature of the sample being analyzed can be obtained as a function of time. In absence of contamination, trace element count rate measured by LA-ICP-MS remained roughly constant during ablation, suggesting a homogeneous 'vertical' distribution of trace elements. This supports that equilibrium or near-equilibrium conditions were achieved in the experiments.

In addition, although we have not analyzed the run products for their water contents, the following procedures help in ensuring that these experiments were anhydrous or nearly so: (1) before putting the dried (at 250°C) Pt-capsule containing the doped starting material in the assembly, all the assembly parts were fired at 1000°C for one hour; (2) just before running the experiment, the entire constructed assembly was kept at 110°C for over 12 hours, and thus we made sure that the assembly was nominally dry or nearly so; and finally (3) pyrophyllite was not used as a gasket material, in the experiments reported here. Pyrophyllite, which is perhaps the biggest source of water was used in the experiments of Canil and Scarfe (1990); Dalton and Presnall (1998a, 1998b), and Gudfinnsson and Presnall (2003, in press). Dalton and Presnall (1998b) analyzed two of their run products, reported 0.31–0.54 wt% water. This amount of water, they argued, was unlikely to have a significant effect on phase

relations and melt compositions. Thus, on this basis, it appears that our experiments were nearly anhydrous.

5. PHASE RELATIONS AND MAJOR ELEMENT COMPOSITIONS

In all, nineteen experiments were performed, but only two that produced clinopyroxenes larger than 15 μm were used for LA-ICP-MS analyses. Other experiments at pressures that ranged from 3 to 6 GPa reproduce the phase equilibria established earlier by Dalton and Presnall (1998a, 1998b) and Gudfinnsson and Presnall (2003, in press). In both cases, quenched liquid occurs as a separated volume located at the top of the charge. However, closer inspection reveals that liquid also occurs at the bottom of the charge. This indicates that the temperature profile within the capsule is slightly saddle-shaped with a shallow thermal minimum in the center of the charge. Overall, the texture of the quench phase separated from crystalline solids is similar to the carbonatitic melt in the experimental products of Gudfinnsson and Presnall (in press). However, compared to past studies, where quenched liquid appeared to be more heterogeneous in being a more complex intergrowth (and more coarse-grained) of carbonate-silicate matrix, the quenched liquid in the experiments reported here, is more uniform in its appearance (Fig. 3).

The crystalline solids, olivine and cpx, are subhedral in outline, and range from $\sim$ 7–30 μm and $\sim$ 20–50 μm, respectively (Fig. 3). In places, tiny (5–10 μm) olivine inclusions are seen near the grain boundaries of cpx. At both the temperatures, olivine in this set of experiments has elevated calcium contents (Table 2), consistent with equilibration with a Ca- and CO_2-rich melt. No major-element zonation can be detected with the electron microprobe. Increasing temperature does not have a marked effect on the CaO content of these olivines. On the other hand, in terms of CaO, MgO, and Al_2O_3, clinopyroxenes show a dramatic change. With increasing temperature, cpx becomes more magnesian, significantly less calcic, and less aluminous (Table 2). Due to the increased MgO and lower Al_2O_3 contents, the higher temperature cpx also has lower calcium-Tschermaks (CaTs) component. The high Al_2O_3 content of cpx in our experiments can be ascribed to the absence of garnet as a crystalline solid. However, the cpx compositions are within the accepted values for the generation of kimberlitic melts in the mantle (Canil and Scarfe, 1990; Dalton and Presnall, 1998b; Gudfinnsson and Presnall, 2003, in press), and thus are of direct relevance to modeling the generation of these CO_2-rich melts.

Compared with the solidus melts coexisting with the garnet lherzolite phase assemblage in the CMAS-CO_2 system at 6 GPa (Dalton and Presnall, 1998a; Gudfinnsson and Presnall, 2003, in press), the melts in this study are enriched in MgO, Al_2O_3, and SiO_2, and poorer in CaO and CO_2, at temperatures above the CO_2-bearing solidus. The melts are still very CO_2-rich, and strongly silica-undersaturated. The compositional evolution of melts with increasing temperature at 6 GPa is very similar to that reported by Dalton and Presnall (1998b) and Gudfinnsson and Presnall (2003, in press). With a temperature increase of only 20°C, the melts show drastic changes in their CaO, MgO, and CO_2 contents, while not showing an appreciable change in SiO_2 and Al_2O_3. With increasing temperature, the melts become significantly more magnesian, less calcic, and also less carbonated. However, at the 6 GPa isobar, while the Mg/Ca ratio (1.04) of the melt at 1430°C in this study agrees well with that of 1380°C (1.03) of Dalton and Presnall (1998b), the Mg/Ca ratio at 1410°C (0.75; this study) is more in line with being "carbonatitic," when compared to the 1380°C (0.74) of Dalton and Presnall (1998a). The reasons for this apparent discrepancy are not clearly understood at present, but increased variance in our study compared to the previous studies could explain these differences, and thus it appears that kimberlitic melts could be produced in equilibrium with cpx of different compositions, and over a considerable temperature range. However, on the basis of melt compositions reported in this study, and their broad, overall agreement with those reported earlier, we conclude that the reported melt compositions here are kimberlitic in nature, and also resemble those of Group IB kimberlites (Smith et al., 1985). Group IB kimberlites have an average Mg/Ca ratio of 2.3, average SiO_2 content of 26 wt%, and are the most CO_2-rich kimberlite group, with an average CO_2 content of 9 wt% (Smith et al., 1985). The higher CO_2 content of the melts reported here compared with the Group IB kimberlites, may thus reflect some degassing of the ascending kimberlite magmas, which has been experimentally demonstrated by Brey et al. (1991).

Combined with the trace element partitioning data (presented later), the similarity in melt compositions reported here to Group I kimberlites (Smith et al., 1985), our experiments are therefore of direct relevance to the petrogenesis of CO_2-rich melts in the mantle. In addition, with further decrease in temperature ($\sim$ 1350°C) the 6 GPa melt compositions (not reported here) become carbonatitic, i.e., $<$ 10 wt% SiO_2, $>$ 30 wt% CaO, $<$ 1 wt% Al_2O_3, 18–20 wt% MgO, and $>$35 wt% CO_2. The present set of experiments combined with those conducted in the past demonstrates that there is essentially a continuum from carbonatitic to kimberlitic melt compositions.

6. TRACE ELEMENT PARTITIONING

6.1. Results from this Work and Comparison with Literature Data

Trace element concentration in cpx and coexisting melts, and corresponding partition coefficients ($D_i^{cpx/melt} = X_i(cpx)/X_i(melt)$, where X_i is the weight fraction of element i) are reported in Table 3. Ordered according to charge and size, partition coefficients from this study and from the literature are plotted in Figure 4. With the exception of Al, Mg, Si, and Ga, the rest of the elements are incompatible in cpx. The D values of Ga are below and above unity at 1430 and 1410°C, respectively. Partition coefficients show a considerable range in magnitude, from $\sim 10^{-3}$ for D_U and D_{Ba} to $\sim$2.5 for D_{Si}. The two experimental runs show similar overall partitioning patterns, D values being lower at 1430°C (Fig. 4a). Rare earth elements (REE) display a wide range of partition coefficients, D_{La} (0.012–0.026) being approximately one order of magnitude lower than D_{Lu} (0.18–0.23).

Partition coefficients for Rb, the only 1+ cation considered in this study, are very similar to those reported previously (Fig. 4b). The upper bound value obtained at 1410°C is in agreement with previous determinations (Green et al., 1992; Blundy and

Table 3. Trace element compositions of the run products and partition coefficients. *n* Number of analyses. Nernst partition coefficients for trace elements (this table) and major elements (Table 2).

Run No.	PR-168		PR170	
P (GPa)	6		6	
T (°C)	1430		1410	
ppm	Qnch (8)	Cpx (4)	Qnch (8)	Cpx (3)
Sc	73.3 (8)	35.5 (22)	76.9 (17)	68.2 (67)
Ga	38.7 (23)	20.7 (14)	7.0 (6)	7.8 (7)
Rb	438.9 (374)	7.1 (9)	471.4 (263)	<5.8
Sr	117.4 (27)	5.8 (3)	159.3 (110)	10.6 (6)
Y	41.9 (13)	6.2 (6)	47.4 (3)	10.9 (11)
Zr	104.6 (40)	1.6 (2)	181.2 (107)	10.4 (31)
Nb	72.6 (13)	0.4 (0)	80.2 (34)	<0.5
Ba	386.7 (148)	0.8 (2)	445.9 (131)	<1.2
La	92.4 (29)	1.1 (1)	106.0 (47)	2.7 (2)
Ce	80.63 (32)	0.8 (1)	94.5 (50)	3.8 (5)
Nd	48.1 (30)	1.5 (1)	61.3 (27)	4.3 (4)
Sm	39.2 (22)	3.2 (4)	48.6 (19)	6.8 (14)
Yb	37.5 (22)	6.7 (7)	44.8 (18)	9.8 (13)
Lu	35.6 (8)	6.4 (6)	40.9 (15)	9.2 (11)
Hf	41.5 (58)	1.4 (0)	43.2 (31)	5.7 (17)
Ta	62.3 (23)	<0.2	68.4 (45)	0.4 (1)
Pb	364.3 (219)	4.7 (3)	15.9 (14)	<1.9
Th	389.8 (194)	0.4 (1)	431.0 (259)	2.5 (6)
U	405.9 (170)	0.2 (1)	461.9 (192)	2.4 (12)
Partition coefficients				
Si	2.50 (1)[x]		2.46 (2)	
Al	1.15 (6)		1.38 (6)	
Mg	1.09 (1)		1.00 (1)	
Ca	0.66 (1)		0.79 (1)	
Sc	0.48 (3)		0.88 (8)	
Ga	0.53 (5)		1.10 (9)	
Rb	0.016 (2)		<0.01	
Sr	0.050 (2)		0.066 (7)	
Y	0.15 (2)		0.23 (3)	
Zr	0.016 (2)		0.057 (16)	
Nb	0.0052 (5)		<0.006	
Ba	0.0020 (4)		<0.003	
La	0.012 (1)		0.026 (2)	
Ce	0.010 (1)		0.040 (5)	
Nd	0.031 (4)		0.071 (7)	
Sm	0.082 (12)		0.14 (3)	
Yb	0.18 (3)		0.22 (3)	
Lu	0.18 (2)		0.23 (3)	
Hf	0.035 (7)		0.13 (4)	
Ta	<0.0035		0.0051 (5)	
Pb	0.013 (1)		<0.12	
Th	0.0019 (2)		0.0058 (13)	
U	0.00060 (34)		0.0052 (22)	

[x] Values in parentheses are two standard errors in terms of least units cited.

Dalton, 2000; Adam and Green, 2001), whereas the value at 1430°C is slightly higher. For the 2+ cations, the partition coefficients decrease with increasing size. A good agreement is found for D_{Mg}, D_{Ca}, and D_{Sr} from this study and the literature. The values of D_{Ba} and D_{Pb} from the literature cover a range of more than two orders of magnitude. In this study, we obtained intermediate value for D_{Ba} (~0.002) and D_{Pb} (~0.013). As shown in Figure 6, the D values for the trivalent cations (3+) gradually decrease from D_{Al} to D_{La} with increasing size by about two orders of magnitude. The values of D_{Al}, D_{Lu}, and D_{Yb} are similar at 1410 and 1430°C. However, Ga, Sc, Y, Sm, Nd, and La clearly have higher D values at lower temperature. At 1430°C, D_{La} is surprisingly higher than D_{Ce}. The reason for this anomaly is not well understood at present. Some melt contamination of cpx analyses may have lead to the observed D values. Our data for 3+ cations best agree with that of Green et al. (1992); Jones et al. (1995), and Adam and Green (2001). The D values reported by Blundy and Dalton (2000) and Klemme et al. (1995) for the 3+ cations lie up to one order of magnitude higher than those from this study. The reasons for this discrepancy are discussed in section 6.2. D values for the 4+ cations, as observed for the 2+ and 3+ cations, decrease with increasing size, except for Th, which has a D slightly higher than D_U (Fig. 4). The origin of this apparent discrepancy is also discussed in section 6.2. The values of D_U and D_{Th} at 1410°C in this study are virtually identical to those of Jones et al. (1995) for augite at 1200°C and 5.5. GPa. However, U and Th are less compatible at 1430°C (Fig. 4), with D_U/D_{Th} a factor of 3 higher at 1430°C (0.89 ± 0.49) than at 1410°C (0.31 ± 0.19). Of studies pertaining to crystal-CO_2-rich melt partitioning, this study reports the lowest values of D_{Hf} and D_{Zr}, D_{Zr}/D_{Hf} being similar at both temperatures (0.44 ± 0.19 at 1410°C and 0.45 ± 0.09 at 1430°C). As expected from size and charge considerations, both Nb and Ta are similarly incompatible in cpx. The partition coefficient of Nb in this study agrees with D_{Nb} reported by Jones et al. (1995), but is lower by a factor of ~2–3 from that of Adam and Green (2001) and Blundy and Dalton (2000) and at least an order of magnitude lower from the values reported by Klemme et al. (1995; Fig. 4b). Differences in D_{Ta} from this study and the studies from Green et al. (1992) and Klemme et al. (1995) are substantial, and we report the lowest values of D_{Nb} and D_{Ta}.

6.2. Factors Controlling the Partitioning

Trace element partitioning between a mineral and melt is primarily a function of phase composition, pressure, and temperature. To properly assess the relative contributions of these influential parameters, it is necessary to isolate their effects from one another. Unfortunately, this has remained problematic because, generally, it is not possible to vary one parameter while keeping the others constant. Variations in pressure and/or temperature conditions are combined with changes in crystal and/or melt compositions. In this section, we use our data and data from the literature to discuss the factors controlling partitioning of trace elements, entering the large M2-site of clinopyroxene.

6.2.1. Lattice strain in clinopyroxene

At a fixed temperature, pressure and phase composition, partition coefficients for a suite of isovalent cations entering a particular mineral lattice site show a near-parabolic dependence on ionic radius centered on r_0, an 'optimum radius' (e.g., Onuma et al., 1968). Theoretical consideration of lattice strain (Brice, 1975; Blundy and Wood, 1994) has helped understand the influence of crystal chemistry on trace element partitioning. In the lattice strain model (Blundy and Wood, 1994), the partitioning of an ion i (D_i) onto a given crystal site is a function of the site elasticity (Young's modulus E), the site size (optimum radius r_0), and the partition coefficient of a cation of

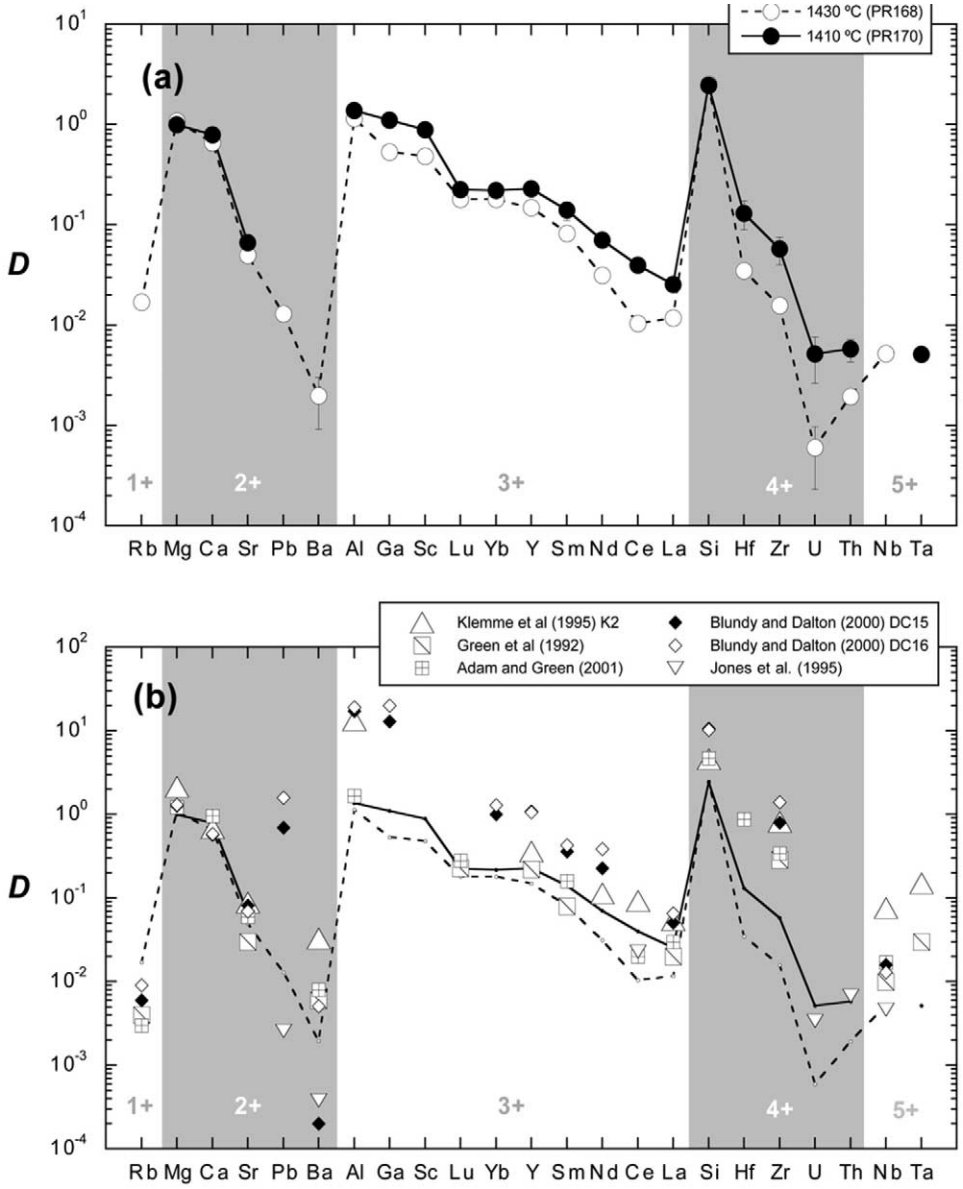

Fig. 4. Cpx–melt partition coefficients ordered according to the charge and size of the cations. (a) Data from this study. (b) Comparison with literature data in CO_2-bearing compositions.

the same charge and of radius r_0 that enters the lattice without strain (optimum partition coefficient D_0):

$$D_i = D_0 \exp\left\{ \frac{-4\pi E N_A}{RT} \left[\frac{r_0}{2}\left(r_i - r_0\right)^2 + \frac{1}{3}\left(r_i - r_0\right)^3 \right] \right\} \quad (1)$$

where N_A is the Avogadro's number, R is the gas constant, and T is the temperature in Kelvin. As shown in Figure 5, the relative compatibilities of 2+ and 3+ cations entering the M2-site are consistent with the effects of lattice strain energy. Similar 'parabolae' are obtained for our two runs at 1410°C (PR170) and 1430°C (PR168). As mentioned in the previous section, the order $D_U < D_{Th}$ is at odds in the sense that, for a given charge D does not decrease with increasing radius, contrary to what can be seen for 2+, 3+, and the other 4+ cations. This observation illustrates one of the effects that crystal chemistry/structure can have on partitioning. Namely, the order $D_U < D_{Th}$ is probably the result of Th and U entering the large M2-site and being located on the left side of the hypothetical 4+ 'partitioning parabola', i.e., we have ${r_0}^{4+M2} > r_{Th} > r_U$. Similarly, from size considerations it is probable that Zr and Hf predominantly enter the smaller M1-site, with Zr and Hf being located on the right side of the 'partitioning parabola', i.e., ${r_0}^{4+M1} < r_{Hf} < r_{Zr}$. Other observations that can be explained by crystal lattice strain are the larger D values obtained for Si and the 3+ cations Al, Ga, and Sc. Theses cations enter different sites than the other cations of the same charge. Si is present only in the small tetrahedral site, whereas Ga and Sc enter predominantly the M1-site. Al is present in both tetrahedral (T-site) and M1-site.

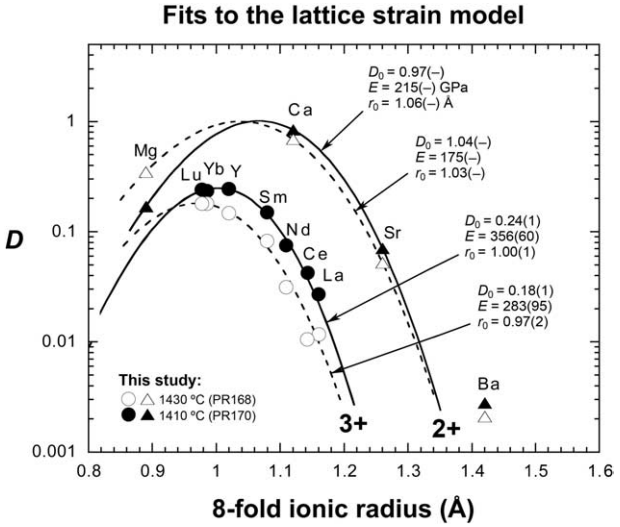

Fig. 5. Partition coefficients for the 2+ and 3+ cations entering the large M2-site as a function of ionic radius. Lines are best fits to the lattice strain model (see Eqn. 1 in the text) using a Levenberg-Marquardt-type, non-linear least squares fitting routine (Press et al., 1992). Note the variations of fit parameters with charge and experimental conditions. Mg in M2-site is calculated from the structural formulae in Table 2. Ionic radii are taken from Shannon (1976). Due to potential melt contamination of the cpx crystals (which would affect only the highly incompatible elements), La, Ce and Ba were not used in the fitting procedure.

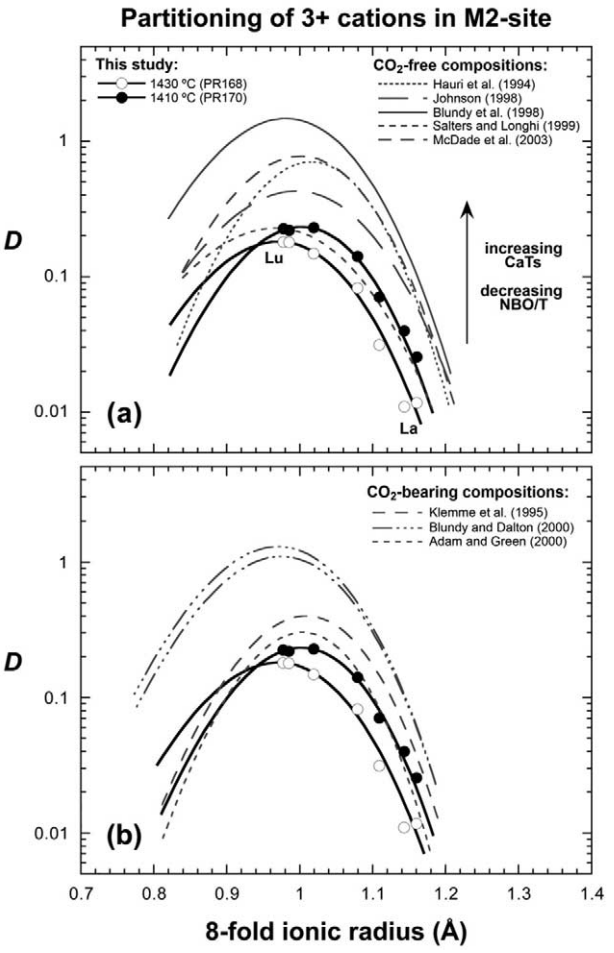

Fig. 6. Fits to REE partition coefficients from this study and (a) CO_2-free compositions, (b) CO_2-bearing compositions. Data sources are: Hauri et al. (1994)—run at 1430°C/2.5 GPa; Salters and Longhi (1999)—run MO1295—3; Klemme et al. (1995)—run K2; Blundy and Dalton (2000)—runs DC15 and DC16. See text for further discussion.

As parabolae for the 2+ and 3+ cations entering the M2-site have been well defined in this study and the literature, we now focus on factors controlling the incorporation of these elements. As shown in Figure 5, we observed that r_0 decreases and E increases with increasing charge of the substituting cation. This is in agreement with previous partitioning studies (e.g., Hill et al., 2000). Looking into more details, it appears that for a given charge: E (1430°C) < E (1410°C), r_0 (1430°C) < r_0 (1410°C), and D_0 (1430°C) < D_0 (1410°C), these changes being more important for the 3+ cations than the 2+ cations. As we performed experiments at a single pressure of 6 GPa, the change of parabolae between our two experiments cannot be due to the effect of pressure. As mentioned earlier, the 20°C difference between runs PR168 and PR170 affects both the clinopyroxene and melt composition, with the CaTs component of the cpx varying from 10 to 8 mol% and Mg/Ca ratio of the melt varying from 0.75 to 1.04. There is evidence that increasing the CaTs content of clinopyroxene increases D values for REE and other elements (e.g., Gaetani and Grove, 1995; Lundstrom et al., 1998; Hill et al., 2000). A high CaTs content should lead to higher D values for 3+ and 4+ cations entering the M2-site due to the charge deficit left by substituting Al for Si. Similarly, more Al substituting for Si should increase the D for the 3+, 4+, and 5+ cations entering the M1-site. This interpretation is consistent with our observation of elevated partition coefficients of REE, Ga, Sc, U, Th, Hf, and Zr for run PR170 compared to run PR168. The 2+ cations are less affected by the combined change of composition and temperature. The values of ${D_0}^{2+M2}$ values derived for both the experiments are almost identical. The main change concerns ${D_{Mg}}^{M2}$, which is higher by a factor of 2–3 at 1410°C. As a consequence, ${E}^{2+M2}$ and ${r_0}^{2+M2}$ are smaller at 1410°C. In comparison to the cpx at 1410°C, the one at 1430°C contains less Ca but more Mg in the M2-site and more Al in both M1-site and T-site (thus higher CaTs component). Therefore, due to the relative size of these host cations, we expect and observe r_0 at 1410°C to be larger than at 1430°C. This interpretation is in agreement with the observation made by Hill et al. (2000) that r_0 decreases with increasing CaTs component of cpx.

6.2.2. *Composition and structure of the melt*

The lattice strain model accords no significance to the melt phase because the latter has negligible elastic strains compared to crystals. However, partitioning experiments between immiscible silicate and carbonate melts (e.g., Jones et al., 1995) and between forsterite and silicate melts (Kohn and Schofield, 1994) have shown that melt composition could contribute to the partitioning of trace elements. There is evidence that a slight change of melt composition can have a large effect on cpx-melt partitioning at very high degree of melt polymerization (e.g., Gaetani and Grove, 1995; Gaetani, 2004). Calculation of the

ratio of non-bridging oxygens to tetrahedrally coordinated cations (NBO/T) is commonly used to provide a measure of the effect of melt structure. Unfortunately for CO_2-bearing melts like the ones of this study, the calculation of NBO/T is inappropriate. Qualitatively, because of their low SiO_2 contents, carbonatitic and kimberlitic melts are likely to be depolymerized melts. Therefore, if we consider the observations made in earlier studies the effect of melt structure is likely to be minor.

6.2.3. *Pressure and temperature*

The effects of pressure on the trace element partitioning cannot be evaluated, as the experiments reported here, were performed only at 6 GPa. The temperature variation in our experiments is relatively small and it is not clear whether temperature has a direct impact on the partitioning. Variations of *D* values can be explained by only variations in the cpx composition and possibly melt composition. To further investigate the potential effects of pressure and temperature, we use a compilation of data from the published literature for the 3+ cations entering the M2-site. Comparison with the published data for CO_2-free and CO_2-bearing compositions, is presented in Figure 6. The partitioning values for the 3+ cations entering the M2-site of clinopyroxene obtained in the present set of experiments are on the low end of the compilation of data for CO_2-free compositions, up to one order of magnitude below the data published by Blundy et al. (1998). As mentioned by Gaetani (2004), the high partition coefficients of Blundy et al. (1998) are probably due to the highly polymerised nature of the silicate melt (NBO/T $\sim$ 0.4). For similar experimental conditions (i.e., clinopyroxene CaTs content, *P* and *T*), McDade et al. (2003) obtained *D* values that are significantly lower with a more depolymerized melt (NBO/T $\sim$ 0.7), close to the *D* values published by Hauri et al. (1994). The data of Johnson (1998) are intermediate between our data and those of Hauri et al. (1994) and McDade et al. (2003), as expected from the relative values of NBO/T and CaTs content. The *D* data in this study are best matched by those from Salters and Longhi (1999) obtained at 2.8 GPa, 1530°C for clinopyroxene with low CaTs content (9 mol%) and relatively depolymerized melt (NBO/T $\sim$ 1.1). Therefore, from Figure 6a and considerations outlined above, it appears that the CaTs content of clinopyroxene and the melt composition/polymerization are the two dominant factors that control the partitioning. At this stage, there is no need to call for direct effects of pressure and temperature to explain variations in *D* values.

In comparison with literature data in CO_2-bearing compositions, a relatively good match is obtained between our data and the data of Adam and Green (2001), and to some extent the data of Klemme et al. (1995; Fig. 6b). In detail, the CaTs component in cpx (11 mol%) in the run K2 of Klemme et al. (1995) is similar to the one of run PR170. The difference in partitioning must be due to other factors. The melt appears to be more polymerized in run K2, the (Si+Al)/(Mg+Ca+Na) ratio (network former/network modifier ratio without taking account of CO_2) being almost a factor of 2 lower than in run PR170. As argued above, higher melt polymerization should *increase* not decrease the *D* values. Therefore, this could mean that pressure and/or temperature, which are lower in run K2 (2 GPa, 1100°C) than in run PR170, may have a non-negligible effect on partitioning. However, the effects of CO_2 and other C species on melt structure are ambiguous at this time, carbonate being seen as both network former and network modifier (R.A. Brooker, 2004 pers. comm.). It is possible that the larger CO_2 content of run K2 leads eventually to a higher degree of polymerization of the melt in comparison with run PR170. The parabolae derived from the data of Blundy and Dalton (2000) at 1375°C are much higher than the ones of this study. This can be explained in terms of higher cpx CaTs content (17 mol%) and possibly higher degree of polymerization if CO_2 acts mainly as network former in the melt. Adam and Green (2001) reported data at 1050°C for cpx with CaTs content (18 mol%) close to the values of Blundy and Dalton (2000). Pressure conditions are only slightly different, 2.5 and 3 GPa, respectively. Major differences concern melt structure and run temperature. Because the CO_2 content in the melt of both studies are approximately similar, the (Si+Al)/(Mg+Ca+Na) ratio can be used with confidence to estimate relative degree of polymerization of the melt. This ratio is lower by a factor of 4 in the runs of Blundy and Dalton (2000), i.e., the melt is more depolymerized in the latter study. Therefore, one should expect lower *D* values in this study if melt structure is the dominant factor. On the contrary, the *D* values are actually *higher* by about a factor of 4. This may indicate that an increase in temperature also increases the REE partitioning in cpx.

To summarize, we found evidence that the composition of cpx and melt (if polymerized), and probably pressure and temperature can have direct effect on partitioning. However, one should remember that the approach we followed above is relatively simplistic given the complexity of the studied systems and the uncertainties on the lattice strain fits. The crystal composition should not be seen as only a matter of CaTs content. The sodium (Na) content of cpx, for example is likely to play a role in charge-balancing the substitution of REE in the M2-site (e.g., Bennett et al., 2004). Runs from Klemme et al. (1995), Blundy and Dalton (2000) and Adam and Green (2001) all contain some Na. Whether Na favors the incorporation of REE via coupled substitution in the M2-site or limits it because Na is a network modifier remains debatable, however. Further experimental work is clearly needed to better constrain the potential effects of composition, pressure, and temperature.

7. GENERATION OF KIMBERLITIC MELTS IN THE EARTH'S MANTLE

Kimberlites, although rare and volumetrically insignificant volcanic rocks, occur almost exclusively in non-orogenic areas of the continents, and the combined studies in geophysics and geochemistry demonstrate that they erupt through thick lithosphere (150–200 km) in a matter of hours or days transversing a vertical distance on the order of tens of kilometers before reaching the surface (Canil and Fedortchouk, 1999). As mentioned earlier, kimberlites have attracted attention largely for bringing diamonds and garnet peridotite mantle xenoliths to the Earth's surface. Furthermore, the suggested derivation of kimberlites from depths greater than any other igneous rock type, and their extreme magma composition (low SiO_2 content and high volatile and trace element contents), makes it important to understand kimberlite petrogenesis, and constrain the melting processes and the composition of the mantle near the cratonic

lithosphere/asthenosphere interface. Kimberlites are never observed as quenched glasses. Instead they contain a variety of macro- and microphenocrysts, often at 10's of volume % abundance that include olivine, calcite, perovskite, serpentine, and minor phlogopite. As opposed to the macrocrystic kimberlites, aphanitic kimberlites have less than 5 vol. % phenocrysts, and are enriched in trace elements by a factor of at least 2–3. They also have higher Ca, Al, and lower Si and Mg contents than "macrocrystic" kimberlites (Bizimis, 2001; le Roex et al., 2003). These variations in mineralogy and major and trace element contents make it difficult to constrain a primary kimberlitic melt composition (Mitchell, 1995; Scott Smith, 1996). On the basis of relative variations in major element compositions between some macrocrystic and aphanitic kimberlites, le Roex et al. (2003) proposed a primary kimberlite magma composition for the Kimberley area (South Africa) that extrapolates to 0.6–0.7% melting of the carbonated lherzolite source suggested by Dalton and Presnall (1998b) and Gudfinnsson and Presnall (2003, in press). On the basis of trace element investigations, it has also been suggested that kimberlites are compatible with 0.4–1.5% melting of a garnet lherzolite source (Fraser and Hawkesworth, 1992; Tainton and McKenzie, 1994; le Roex et al., 2003). To account for the very high incompatible trace element content of the kimberlites, all these studies require a source for the generation of kimberlites that is more enriched relative to the primitive mantle.

As discussed earlier, the experimental compositions and the *P-T* conditions of this study appear suitable for the generation of kimberlitic melts deep in the Earth's mantle. We therefore use the cpx-melt partition coefficients determined in this study to investigate whether they are indeed appropriate for kimberlitic melts and put constraints on the nature of the kimberlite source. The high abundance of phlogopite megacrysts in Group II kimberlites suggests derivation from a hydrous source (Mitchell, 1995). As our data were obtained in a water-free system, this group of kimberlites is not considered in our modeling. We focus only on Group I (GI) kimberlites from the Kimberley area, for which a primary magma composition has been estimated (le Roex et al., 2003).

We model the trace element composition of GI kimberlite melts with a forward incremental melting model of 0.1% melt increments (Bizimis et al., 2000, in press) using the cpx-melt partition coefficients obtained in this study. On the basis of the phase assemblage of a carbonated mantle at 6 GPa (Dalton and Presnall, 1998b; Gudfinnsson and Presnall, 2003, in press; this study), melting takes place exclusively in the garnet lherzolite stability field. Unfortunately, there are no garnet-melt partition coefficients available for the CO_2-bearing compositions. However, due to the similarity of *D* values of cpx between this work and Salters and Longhi (1999) and Salters et al. (2002), it appears that the *D* values of garnet coexisting with cpx at 2.8–3.4 GPa of Salters and Longhi (1999) and Salters et al. (2002) can be used, at least as a first approximation, in the modeling presented here. For consistency, we also use the *D* values of orthopyroxene (opx) and olivine from Salters and Longhi (1999) and Salters et al. (2002), respectively. When not available in the latter studies, some *D* values were obtained either by interpolation from the neighboring elements or from other studies (see references). The partition coefficients used in the numerical models are listed in Table 4. The model source compositions and melting reactions are taken from Salters and Longhi (1999; Table 4) and are appropriate for high-pressure mantle compositions (2.8–3.4 GPa). Due to the low degree of melting used in our calculations (0.5%–1%; see the discussion later) and also because of the relatively large abundance and starting source composition, the most important factors controlling the melt composition are the partition coefficients for cpx, while the melting reactions have only a minor effect. Our numerical experiments suggest that using either the melting reactions of Walter (1998) for melting of anhydrous garnet lherzolite at 7 GPa (which has a melt fraction of opx entering the melt at 0), or the melting reactions of Dalton and Presnall (1998a, 1998b) for a carbonated garnet lherzolite at 6 GPa, gives results that are indistinguishable from the results shown in Figure 7.

The relatively radiogenic Nd and unradiogenic Sr isotope compositions of South African GI kimberlites (Smith, 1983) suggest that their source has experienced a long-term depletion relative to a chondritic Earth. Therefore, for our model, we use as a starting composition a depleted mantle source (i.e., mid-ocean ridge basalt, MORB; Salters and Stracke, 2004). Any other depleted (e.g., some ocean-island basalts or continental volcanics) source could be used, but on the basis of relative uniformity of MORB compositions compared to ocean-island basalts (OIB) and continental volcanics we choose the better-constrained MORB reservoir source as a dominant "tank" in the upper mantle. We compare the trace element compositions of our modeled melts with the GI kimberlite compositions from Kimberley (le Roex et al., 2003). The results of our modeling using the above-mentioned parameters are shown in Figure 7. For clarity, we show two compositions that essentially cover the range of these GI kimberlites (Fig. 7): one is sample COL1, similar to a proposed primary kimberlite magma (le Roex et al., 2003), and the other sample, K5/94, represents the most trace element enriched aphanitic kimberlite from the Wesselton Sills (le Roex et al., 2003). The aphanitic Wesselton Sills kimberlites have been suggested to represent products of extreme fractionation of a primary kimberlitic magma (le Roex et al., 2003). It can be seen that a small (0.5 wt%) degree melt from a depleted mantle source (similar to a MORB source) does not resemble the trace element compositions of the sampled GI kimberlites. Relative to the kimberlite sample, the light rare earth element to the heavy rare earth element ratios (LREE/HREE) is too low. The highly incompatible element Ba, Th, U, Nb, and Ta concentrations are also too low in the modeled melts. Our model calculations therefore suggest that a depleted mantle source (similar to the MORB source) is too depleted in most of the highly incompatible elements, to give rise to the observed trace element concentrations in the natural samples of kimberlites. Thus, it appears that a more enriched source is needed to "satisfy" the trace element budget of natural kimberlites. However, such an enriched source cannot be a primitive mantle-like source, as it also must satisfy the long-term depletion constraints imposed by the Nd and Sr-isotope data on the GI kimberlites. In the following section, we try to constrain the composition and longevity of such an enriched source.

Our numerical experiments show that a source capable of generating kimberlite-like trace element compositions can be produced by metasomatism of a depleted mantle source by melts generated from the same mantle source (Table 4). In a

Table 4. Mineral-melt partition coefficients used in this study.

Element	Cpx (1430°C)	Opx[a]	Olivine[a]	Garnet[a]	GI source (ppm)[c]
Ba	0.00208	0.001	0.0001	0.0006	4.18–7.16
Th	0.00195	0.0009	0.00005	0.010	0.047–0.0816
U	0.00060	0.00315	0.00005	0.0276	0.0158–0.027
Nb	0.00520	0.0033	0.0004	0.0171	0.707–1.20
Ta	0.00350	0.0049	0.0004	0.017	0.0465–0.079
La	0.01230	0.001	0.0001	0.005	0.801–1.367
Ce	0.0100	0.0039	0.0003	0.0201	2.5–4.22
Pb	0.0130	0.009	0.0035	0.005	0.069–0.115
Sr	0.0500	0.003	0.001	0.01	25.6–41.5
Nd	0.0310	0.012	0.001	0.0939	1.58–2.44
Zr	0.0160	0.01667	0.0033	0.5648	14.1–18.3
Hf	0.0350	0.033	0.001	0.597	0.274–0.348
Sm	0.0820	0.019	0.001	0.331	0.408–0.546
Eu	0.1	0.03	0.0015	0.5	0.146–0.1853
Ti	0.15	0.112	0.0281	0.305	1012–1226
Y	0.1500	0.0455	0.0099	3.046	4.34–4.60
Er	0.182	0.0717	0.0132	3.441	0.391–0.411
Yb	0.1800	0.1013	0.0305	5.724	0.41–0.42
Lu	0.1800	0.127	0.043	7.409	0.064–0.0647

Source mineral mode[b]

	Olivine	Opx	Cpx	Garnet
Melting mode[b]	0.62	0.15	0.15	0.08
	0.028	−1.18	1.66	0.492

[a] Average partition coefficients for garnet and orthopyroxene (opx) and olivine from Salters and Longhi (1999) and Salters et al. (2002), respectively. D_{Ti} calculated from the major element composition of the phases in these experiments. Other D values approximated from the neighboring elements and for opx from McDade et al. (2003). D_{Eu} approximated from D_{Sm}. $D_{Sr}^{garnet/melt}$ approximated from Pertermann et al. (2004).

[b] Source mineralogy, melting mode, and arguments in favor of 30% modal pyroxene and 8% garnet in the lherzolitic source in this paper are on the basis of Salters and Longhi (1999).

[c] Range of calculated GI source composition product of metasomatism of a depleted mantle source with the addition of 2.5% and 5% melt of a 1% melt from this source (see text for more details).

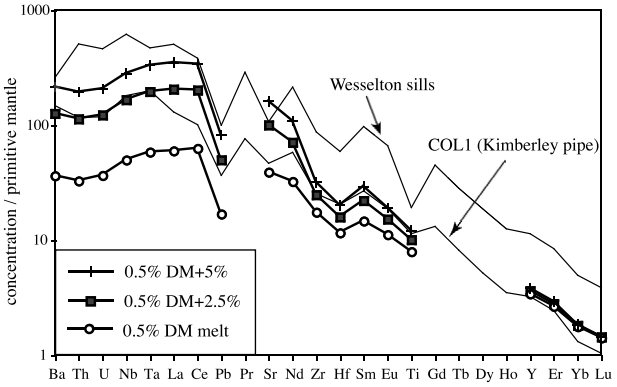

Fig. 7. Primitive mantle normalized concentrations of kimberlites and model melts using the cpx/melt partition coefficients from this study. Primitive mantle values are from McDonough and Sun (1995). *Wesselton Sills* and *COL1* kimberlite samples essentially cover the range of GI kimberlite concentrations from Kimberley field (le Roex et al., 2003). Three model melt compositions are shown: *0.5% DM melt* = 0.5% melt from a depleted mantle source (MORB source; Salters and Stracke, 2004). *0.5% DM + 2.5%* = 0.5% melt from a depleted mantle source that is metasomatised by the addition of 2.5% of 1% melt from such a depleted MORB source. *0.5% DM + 5%* = same as before, but the depleted source is metasomatised by the addition of 5% of 1% melt from a depleted source.

sense, this is a type of "self-metasomatism" process where small degree melts, that are generated from a depleted mantle (relative to a chondritic Earth) are being trapped and then freeze within a similar (compositionally) mantle source, creating a relatively enriched source. In Figure 7 we show two model melts generated by 0.5% melting of such an enriched mantle source. This source is the product of addition of 2.5 and 5% (by weight) of a 1% melt to the depleted mantle source. In terms of the LREE/HREE slope, the Zr, Hf, and Ti depletions relative to the neighboring REE, the negative Pb depletion, and the Ba to Ta range, these model melts resemble remarkably well the sampled kimberlites (Fig. 7). Also, assuming a CO_2/Nb ratio of 230 ± 55 for the depleted mantle (Salters and Stracke, 2004), and similar incompatibility of CO_2 as Nb, taken from the near constant ratio of CO_2/Nb in primitive melt inclusions (Saal et al., 2002), the model kimberlite melt will have ~ 2 to 3 wt% CO_2, which is on the low end of the kimberlite compositions (le Roex et al., 2003). Similarly, on the basis of H_2O/Ce ratio of 168 ± 95 for the depleted mantle (Salters and Stracke, 2004), the model kimberlite melt reported here will have ~ 4.5% H_2O, and a H_2O/CO_2 ratio of ~ 1.5, which is essentially identical to the average H_2O/CO_2 ratio of ~ 1.41 in the GI kimberlites reported by le Roex et al. (2003).

Our melting calculations show that with increasing melt addition to the metasomatised source, the melts from this source (i.e., kimberlite model melts) become progressively

LREE enriched, but at nearly constant HREE contents. In fact, any changes either in the amount of melt addition to the depleted source or the degree of melting of such metasomatised source results in significant changes in the highly incompatible element concentrations, while the more compatible HREE, due to their high partition coefficients in garnet, stay essentially constant. These calculations suggest that the near parallel patterns of the two plotted kimberlites (and the rest of the Kimberley GI kimberlites) cannot be reconciled with variable degrees of melting and/or source enrichment in the kimberlite source. These parallel trace element patterns more likely result from a combination of fractionation and/or assimilation of mantle peridotite (e.g., le Roex et al., 2003). However, our modeling shows that the experimentally produced cpx-melt partition coefficients in this study are appropriate for generating kimberlite-like trace element compositions (LREE/HREE ratios, Zr-Hf-Ti and Pb depletions, as well as volatile contents) from a mantle source similar to MORB source, through an enrichment process that involves melts from within the same source.

The notable exceptions of our model fit to the natural data are La, Ce, and Sr. Relative to Nd, Sr depletion in kimberlites cannot possibly be generated from any normal mantle source (i.e., depleted or primitive mantle and their derivatives through melt metasomatism), with the available partition coefficients: Sr is always more incompatible than Nd in both cpx and garnet (Hauri et al., 1994; Johnson, 1998; this study). This observation requires some mechanism other than melting of a typical mantle mineralogy that must decouple Sr from the REE in the mantle. Phlogopite or amphibole that do have higher D_{Sr} than D_{Nd} (Foley et al., 1996) are not expected to be residual minerals in the GI source, because Nb and Ta with high D values in phlogopite and amphibole are not depleted in GI kimberlites (see also discussion by le Roex et al., 2003). Since a carbonate phase is stable at the CO_2-bearing lherzolite solidus for the small degrees of melting used here (Dalton and Presnall, 1998b; Gudfinnsson and Presnall, 2003, in press), it is conceivable that if such carbonate does remain residual during the kimberlite melting event, then the observed Sr depletion in kimberlites can be generated by the presence of only 1% modal carbonate, in this source, with the conservative assumption that $D_{Sr}^{carbonate/melt} = 1$. We are not aware of any experimentally determined carbonate/melt partition coefficients for Sr, but evidence from carbonates in mantle xenoliths (Lee et al., 2000) suggests that primary mantle carbonates have very high Sr and very low Nd concentrations suggesting a preferential partitioning of Sr over Nd in a mantle carbonate. Therefore, if small amounts ($< 1\%$) of a carbonate mineral phase remain residual during kimberlite melting, this could explain the relative Sr depletions in kimberlites.

As mentioned earlier, the depleted Nd and Sr isotope compositions of the GI kimberlites require a long-term depleted mantle source, relative to a chondritic earth. However, our model calculations require that such a source must be enriched relative to a depleted MORB-like source to produce kimberlitic melts. We use the GI source Sm/Nd ratio ($^{147}Sm/^{144}Nd = 0.156$) estimated from our model and an average Nd isotope composition of the GI kimberlites ($^{143}Nd/^{144}Nd = 0.51267$; Smith, 1983) to investigate the longevity of such a source in the sublithospheric mantle. Figure 8 compares the Nd isotopic evolution of the model kimberlite source with the isotopic

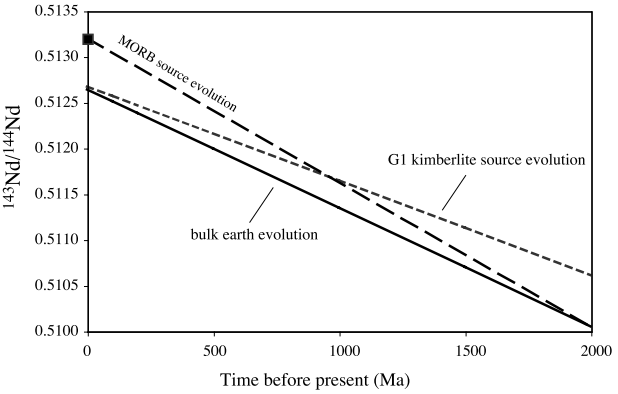

Fig. 8. Nd isotope evolution of the calculated GI kimberlite source, compared with a calculated MORB source and bulk earth evolution. Bulk earth $^{143}Nd/^{144}Nd = 0.512638$ and $^{147}Sm/^{144}Nd = 0.1967$, $\lambda_{Nd} = 6.54*10^{-12}$. Present day MORB source $^{143}Nd/^{144}Nd = 0.5132$, and evolution lines are calculated assuming that the MORB source was generated 2 Ga ago from chondritic earth. GI kimberlite source is taken as $^{143}Nd/^{144}Nd = 0.51267$ (Smith, 1983) and $^{147}Sm/^{144}Nd = 0.156$, from the successful GI source that produces melts with kimberlite-like trace elements (see text and Fig. 8 for details).

evolution of the depleted mantle (taken as the MORB source with an average age of depletion of 2 Ga; Salters and Stracke, 2004) and chondritic earth. The GI source, having subchondritic Sm/Nd ratio, will evolve with a shallower slope than both the MORB source and bulk earth. As the $^{143}Nd/^{144}Nd$ ratio of the GI kimberlites is greater than the bulk earth, the GI source evolution line does not intercept the bulk earth Nd evolution line, but a more depleted source. Figure 8 shows that the model GI source evolution will intersect a 2 Ga old MORB-type source at ~1 Ga. Assuming that MORB-type mantle is the most depleted source of magmas on earth, then this is the oldest age at which the GI source could have existed. If a source less depleted than the MORB source is assumed in all the previous calculations, then the GI source must be younger than the ca. 1-Ga age shown in Figure 8. These calculations are far from being unique but show that, in general, the average age of the GI kimberlite source predicted by our model must be on the order of 1 Ga or younger. This age most likely reflects the average age of a series of metasomatic events that took place over time in the GI source, and may not necessarily have a geologic significance.

The above calculations are by far non-unique, and it is possible that different combination of partition coefficients, source mineralogy, and/or melting reactions can create similar results. However, the combination of our experimentally determined derived cpx-melt partition coefficients coupled with the constraints imposed by the GI kimberlite compositions (derivation from a long-term depleted source, enriched trace element concentrations), show that the GI source can be a depleted, MORB-like reservoir that has been metasomatically enriched by small degree melts from such a source, and that the age of G I source cannot be older than 1 Ga. Our results further suggest that the source of GI kimberlites may occur at the lithosphere-asthenosphere levels. We can envision small degree melts from the asthenospheric mantle that percolate upward and create a metasomatic horizon near the bottom of the non-convecting sublithospheric mantle. Accumulation of such small

degree melts and the presence of volatiles, together with conductive heating may at some point in time trigger melting and lead to subsequent eruption of the kimberlitic melts.

8. CONCLUSIONS

The experimentally produced melts at 6 GPa and 1410 and 1430°C in this study contain ~ 28 wt% dissolved CO_2, and are saturated with olivine and clinopyroxene. With decreasing temperature, melt compositions, while not changing in their SiO_2, Al_2O_3, and CO_2 contents, exhibit an appreciable increase in their CaO and MgO contents. With decreasing temperature, clinopyroxene becomes more calcic, less magnesian, and also less aluminous. With the exception of Al, Mg, Si, and Ga, all elements are incompatible in cpx. Partition coefficients show a considerable range in magnitude, from $\sim 10^{-3}$ for D_U and D_{Ba} to ~2.5 for D_{Si}. The two experimental runs show similar overall partitioning patterns with the D values lower at 1430°C. Additionally, there appears to be a significant difference between $D^{cpx/kimberlite\ melt}$ (this study) and $D^{cpx/basaltic\ melt}$. Also, there are subtle, but significant differences between $D^{cpx/kimberlite\ melt}$ (this study) and $D^{cpx/carbonatite\ melt}$. Indeed, of all the mineral-melt trace element partitioning studies undertaken so far in the carbonated systems, we report the lowest D values. These differences perhaps reflect combined effects of pressure, temperature, and composition. Partition models for the 2+ and 3+ cations, developed on the basis of lattice strain theory, show a near-parabolic dependence on the radius of incorporated cations, further suggesting the important role of crystal chemistry in governing the trace element partitioning, an effect also found in this study. At this stage, it is not entirely clear what the effects of P, T, and melt composition are, on trace element partitioning in carbonated systems.

The partition coefficients obtained in this study were used to model the generation of the Group I (GI) kimberlites. Our calculations show that kimberlitic melts can be produced in the asthenospheric mantle by ~0.5% melting of a MORB-type depleted source that has been enriched by small degree melts originating from a similar depleted source. Additionally, on the basis of D values obtained in this study, we show that the GI source can be generated by a series of metasomatism events of a 2-Ga old MORB-type source ca. 1 Ga ago or later (Bizimis et al., 2005; Goldschmidt, 1937; Lundstrom et al., 1995).

Acknowledgments—SK thanks Dean Presnall for his boundless generosity, both with unpublished data and many ideas, and more importantly for his gentle way of putting up with some thoughts even when he knows they are sordid. This paper is a result of some conversations that SK had with Dean some time ago in Miami, and when Dean commented "It might be fun and useful to explore the element partitioning behavior at high pressures in carbonated mantle to model the generation of CO_2-rich melts, and it is best to start with simple systems as they appear to be well-behaved." On reflection, it was not only fun, but a sound research suggestion too, that allowed SK to learn more about various other forms of phase diagrams in simple systems, and their application to mantle melting. Many thanks, Dean. SK also thanks Steve Haggerty for many discussions on the petrography and geochemistry of kimberlites, sharing his knowledge on kimberlites from around the world, and for commenting, "we should be careful with interpreting the genesis of these messy rocks." Jerry Beavers at the University of Texas at Dallas and Bert Collins and Bobbie Brown at the Geophysical Lab are thanked for machining some of the parts used in these experiments. Thanks to Bjørn Mysen for discussions on the petrogenesis of CO_2-rich melts and also for extending his lab facilities. AC acknowledges Richard Brooker for discussions pertaining to the solubility of CO_2 in melts. The able working of the multi-anvil devices at the Geophysical Lab is due to Chris Hadidiacos and Dave George's skills and tenacity. The authors also thank Richard Ash at the University of Maryland for his able help in acquisition of the laser probe data. Rondi Davies, Steve Haggerty, and Dean Presnall are thanked for their useful comments (at a short notice) on different versions of this paper. Tahar Hammouda and an anonymous referee provided critical reviews that lead (hopefully) to a better presentation. Thanks also to Martin Menzies for handling the paper. The Carnegie Institution of Washington and grants to Yingwei Fei (NASA-NNG04GG09G), Bill McDonough (NSF-EAR 0337621), Jim Van Orman (NSF EAR-0322766), Dean Presnall (NSF EAR-0106645), Gautam Sen and Vincent Salters (NSF-OCE 0241681) supported this research.

Associate editor: M. A. Menzies

REFERENCES

Adam J. and Green T. H. (2001) Experimentally determined partition coefficients for minor and trace elements in peridotite minerals and carbonate melt and their relevance to natural carbonatites. *Eur. Jour. Min.* **13,** 815–827.

Bell K. and Blenkinsop J. (1987) Archean depleted mantle—evidence from Nd and Sr initial isotopic ratios of carbonatites. *Geochim. Cosmochim. Acta* **51,** 291–298.

Bennett S., Blundy J. D. and Elliott T. (2004) The effect of sodium and titanium on crystal-melt partitioning of trace elements. *Geochim. Cosmochim. Acta* **68,** 2335–2347.

Bizimis M., Salters V. J. M. and Bonatti E. (2000) Trace and REE content of clinopyroxenes from Supra-subduction zone peridotites: implications for melting and enrichment processes in the island arcs. *Chem. Geol.* **165,** 67–85.

Bizimis M. (2001) Geochemical processes in the upper mantle: evidence from peridotites, kimberlites and carbonatites. Unpublished PhD Dissertation, Florida State University.

Bizimis M., Sen G., Salters V. J. M. and Keshav S. (in press) Hf-Nd-Sr isotope systematics of garnet pyroxenites from Salt Lake Crater, Oahu, Hawaii: evidence for a depleted component in the Hawaiian volcanism. *Geochim. Cosmochim. Acta*

Blundy J. D. and Wood B. J. (1994) Prediction of crystal-melt partition coefficients from elastic moduli. *Nature* **372,** 452–454.

Blundy J. D., Robinson J. A. C. and Wood B. J. (1998) Heavy REE are compatible in clinopyroxene on the spinel lherzolite solidus. *Earth Planet. Sci. Lett.* **160,** 493–504.

Blundy J. D. and Dalton J. A. (2000) Experimental comparison of trace element partitioning between clinopyroxene and melt in carbonate and silicate systems and implications for mantle metasomatism. *Contrib. Mineral. Petrol.* **139,** 356–371.

Brenan J. and Watson E. B. (1991) Partitioning of trace elements between carbonate melt and clinopyroxene and olivine at mantle P-T conditions. *Geochim. Cosmochim. Acta* **55,** 2203–2214.

Brey G. P., Brice W. R., Ellis D. J., Green D. H., Harris K. L. and Ryabchikov I. D. (1983) Pyroxene-carbonate reactions in the upper mantle. *Earth Planet. Sci. Lett.* **62,** 63–74.

Brey G. P., Kogarko L. N. and Ryabchikov I. D. (1991) Carbon dioxide in kimberlitic melts. *N. J. fur Mineral., Monat.* **4,** 159–168.

Brice J. C. (1975) Some thermodynamic aspects of the growth of strained crystals. *J. Cryst. Gr.* **28,** 249–253.

Canil D. and Scarfe C. M. (1990) Phase relations in the peridotite + CO_2 system to 12 GPa: implications for the origin of kimberlite and carbonate stability in the Earth's upper mantle. *J. Geophys. Res.* **95 B10**, 15805–15816.

Canil D. and Fedortchouk Y. (1999) Garnet dissolution and the emplacement of kimberlites. *Earth Planet. Sci. Lett.* **167,** 227–237.

Dalton J. A. and Wood B. J. (1993) The compositions of primary carbonate melts and their evolution through wall-rock reaction. *Earth Planet. Sci. Lett.* **119,** 511–525.

Dalton J. A. and Presnall D. C. (1998a) Carbonatitic melts along the solidus of model lherzolite in the system CaO-MgO-Al_2O_3-SiO_2-CO_2 from 3 to 7 GPa. *Contrib. Mineral. Petrol.* **131,** 123–135.

Dalton J. A. and Presnall D. C. (1998b) The continuum of primary carbonatitic-kimberlitic melt compositions in equilibrium with lherzolite: data from the system CaO-MgO-Al_2O_3-SiO_2-CO_2 at 6 GPa. *J. Petrol.* **39,** 1953–1964.

Foley S. F., Jackson S. E., Fryer B. J., Greenough J. D. and Jenner G. A. (1996) Trace element partition coefficients for clinopyroxene and phlogopite in an alkaline lamprophyre from Newfoundland by LAM-ICP-MS. *Geochim. Cosmochim. Acta* **60,** 629–638.

Fraser K. J. and Hawkesworth C. J. (1992) The petrogenesis of ultrapotassic group 2 kimberlites from the Finsch Mine, South Africa. *Lithos* **28,** 327–345.

Gaetani G. A. and Grove T. L. (1995) Partitioning of rare earth elements between clinopyroxene and silicate melt: crystal-chemical controls. *Geochim. Cosmochim. Acta* **59,** 1951–1962.

Gaetani G. A. (2004) The influence of melt structure on trace element partitioning near the peridotite solidus. *Contrib. Mineral. Petrol.* **147,** 511–527.

Green D. H. and Wallace M. E. (1988) Mantle metasomatism by ephemeral carbonatite melts. *Nature* **336,** 459–462.

Green T. H., Adam J. and Sie S. H. (1992) Trace element partitioning between silicate minerals and carbonatite at 25 kbar and application to mantle metasomatism. *Mineral. Petrol.* **46,** 179–184.

Gudfinnsson G. H. and Presnall D. C. (2003) Continuous gradations among primary kimberlitic, carbonatitic, melilititic and komatiitic melts in equilibrium with garnet lherzolite at 3–8 GPa. *Proc. 8th Int. Kimber. Conf.* Extended abstracts.

Gudfinnsson G. H. and Presnall D. C. (in press) Continuous gradations among primary carbonatitic, kimberlitic, melilititic, basaltic and komatiitic melts in equilibrium with garnet lherzolite at 3–8 GPa. *J. Petrol.*

Haggerty S. E. (1994) Superkimberlites: a geodynamic window to the Earth's core. *Earth Planet. Sci. Lett.* **122,** 57–69.

Hauri E. H., Shimizu N., Dieu J. J. and Hart S. R. (1993) Evidence for hotspot-related carbonatite metasomatism in the oceanic upper mantle. *Nature* **365,** 221–227.

Hauri E. H., Wagner T. and Grove T. L. (1994) Experimental and natural partitioning of Th, U, Pb, and other trace elements between garnet, clinopyroxene and basaltic melts. *Chem. Geol.* **117,** 149–166.

Hill E., Wood B. J. and Blundy J. D. (2000) The effect of Ca-Tschermaks component on trace element partitioning between clinopyroxene and silicate melt. *Lithos* **53,** 203–215.

Hunter R. H. and McKenzie D. P. (1989) The equilibrium geometry of carbonate melts in rocks of mantle composition. *Earth Planet. Sci. Lett.* **92,** 347–356.

Ionov D. A., Dupuy C., O'Reilly S. Y., Kopylova M. G. and Genshaft Y. (1993) Carbonate peridotite xenoliths from Spitsbergen: implications for trace element signature of carbonate mantle metasomatism. *Earth Planet. Sci. Lett.* **119,** 283–297.

Ionov D. A., O'Reilly S. Y., Kopylova M. G. and Genshaft Y. (1996) Carbonate-bearing mantle peridotite xenoliths from Spitsbergen: phase relationships, mineral compositions and trace element residence. *Contrib. Mineral. Petrol.* **125,** 375–392.

Irving A. J. and Wyllie P. J. (1975) Subsolidus and melting relationships for calcite, magnesite and the $CaCO_3$-$MgCO_3$ to 36 kb. *Geochim. Cosmochim. Acta* **39,** 35–53.

Johnson K. T. M. (1998) Experimental determination of partition coefficients for rare earth and high-field strength elements between clinopyroxene, garnet and basaltic melt at high pressure. *Contrib. Mineral. Petrol.* **133,** 60–68.

Jones J. H., Walker D., Pickett D. A., Murrell M. A. and Beattie P. (1995) Experimental investigation of the partitioning of Nb, Mo, Ba, Ce, Pb, Ra, Th, Pa and U between immiscible carbonate and silicate liquids. *Geochim. Cosmochim. Acta* **59,** 1307–1320.

Klemme S., van der Laan S. R., Foley S. F. and Gunther D. (1995) Experimentally determined trace and minor element partitioning between clinopyroxene and carbonatite melt under upper mantle conditions. *Earth Planet. Sci. Lett.* **133,** 439–448.

Kohn S. C. and Schofield P. F. (1994) The importance of melt composition in controlling trace-element behaviour: an experimental study of Mn and Zn partitioning between forsterite and silicate melts. *Chem. Geol.* **117,** 73–87.

Lee W.-J., Wyllie P. J. and Rossman G. R. (1994) CO_2-rich glass, round calcite crystals and no liquid immiscibility in the system CaO-SiO_2-CO_2 at 2.5 GPa. *Am. Min.* **79,** 1135–1144.

Lee C.-T., Rudnick R. L., McDonough W. F. and Horn I. (2000) Petrologic and geochemical investigations of carbonates in peridotite xenoliths from northeastern Tanzania. *Contrib. Mineral. Petrol.* **139,** 470–484.

le Roex A. P., Bell D. R. and Davis P. (2003) Petrogenesis of Group I Kimberlites from Kimberley, South Africa: evidence from bulk-rock geochemistry. *J. Petrol.* **44,** 2261–2286.

Lundstrom C. C., Shaw H. F., Ryerson F. J., Williams Q. and Gill J. (1998) Crystal chemical control of clinopyroxene-melt partitioning in the Di-Ab-An system: implications for elemental fractionations in the depleted mantle. *Geochim. Cosmochim. Acta* **62,** 2849–2862.

McDade P., Blundy J. D. and Wood B. J. (2003) Trace element partitioning on the Tinaquillo lherzolite solidus at 1.5 GPa. *Phys. Earth. Planet. Int.* **139,** 129–147.

Minarik W. G. and Watson E. B. (1995) Interconnectivity of carbonate melt at low melt fraction. *Earth Planet. Sci. Lett.* **133,** 423–437.

Mitchell R. H (1995) Kimberlites, orangeites and related rocks. Plenum Press.

Nelson D. R., Chivas A. R., Chappel B. W. and McCulloch M. T. (1988) Geochemical and isotopic systematics in carbonatites and implications for ocean-island sources. *Geochim. Cosmochim. Acta* **52,** 1–17.

Onuma N., Higuchi H., Wakita H. and Nagasawa H. (1968) Trace element partition between two pyroxenes and the host lavas. *Earth Planet. Sci. Lett.* **5,** 47–51.

Pearson D. G., Canil D. and Shirey S. B. (2004) Mantle samples included in volcanic rocks: xenoliths and diamonds. In *Treatise on Geochemistry: The Mantle and Core Vol. 2* (ed. R. Carlson), pp. 171–276. Elsevier Pergamon.

Pertermann M., Hirschmann M. M., Hametner K., Gunther D. and Schmidt M. W. (2004) Experimental determination of trace element partitioning between garnet and silica-rich liquid during anhydrous partial melting of MORB-like eclogite. *Geochem. Geophys. Geosys.* **5,** DOI 10.1029/2003GC000638.

Presnall D. C. (1986) An algebraic method for determining equilibrium crystallization and fusion paths in multicomponent systems. *Am. Min.* **71,** 1061–1070.

Press W. H., Teukolsky S. A., Vetterling W. T. and Flannery B. P. (1992) Numerical Recipes in C. 2nd edition, pp. 965. Cambridge University Press.

Rudnick R. L., McDonough W. F. and Chappel B. W. (1993) Carbonatite metasomatism in the northern Tanzania mantle: petrographic and geochemical characteristics. *Earth Planet. Sci. Lett.* **114,** 463–475.

Saal A., Hauri E. H., Langmuir C. H. and Perfit M. R. (2002) Vapor undersaturation in primitive mid-ocean ridge basalt and the volatile content of the Earth's upper mantle. *Nature* **419,** 451–455.

Salters V. J. M. and Longhi J. (1999) Trace element partitioning during the initial stages of melting beneath mid-ocean ridges. *Earth Planet. Sci. Lett.* **166,** 15–30.

Salters V. J. M., Longhi J. and Bizimis M. (2002) Near mantle solidus trace element partitioning at pressures upto 3.4 GPa. *Geochem. Geophys. Geosys.* **3,** DOI 10.1029/2001GC000148.

Salters V. J. M. and Stracke A. (2004) Composition of the depleted mantle. *Geochem. Geophys. Geosys.* **5,** DOI 1029/2003GC000597.

Shannon R. D. (1976) Revised effective ionic radii and systematic studies of interatomic distances in halides and chalcogenides. *Acta Cryst.* **A32**, 751–767.

Smith C. B. (1983) Pb, Sr and Nd isotopic evidence for the sources of South African Cretaceous kimberlites. *Nature* **304,** 51–54.

Smith C. B., Gurney J. J., Skinner E. M. W., Clement C. R. and Ibrahim N. (1985) Geochemical character of southern African kimberlites: a new approach based on isotopic constraints. *Trans. Geol. Soc. S. Africa* **88,** 267–280.

Thibault Y., Edgar A. D., Lloyd F. E. (1992) Experimental investigation of melts from a carbonated phlogopite lherzolite: implications for metasomatism in the continental lithospheric mantle. *Am. Min.* **77,** 784–794.

van Westrenen W., Van Orman J. A., Watson H., Fei Y. and Watson E. B. (2003) Assessment of temperature gradients in multianvil assemblies using spinel layer growth thickness. *Geochem. Geophys. Geosys.* **4,** DOI 10.1029/2002GC0007474.

Wallace M. E. and Green D. H. (1988) An experimental determination of primary carbonatite magma composition. *Nature* **335,** 343–346.

Walter M. J., Thibault Y., Wei K. and Luth R. W. (1995) Characterizing experimental pressure and temperature conditions in multianvil apparatus. *Can. J. Phys.* **73,** 273–286.

Walter M. J. (1998) Melting of garnet peridotite and the origin of komatiite and depleted lithosphere. *J. Petrol.* **39,** 29–60.

Walker D., Beattie P. and Jones J. H. (1992) Partitioning of U-Th-Pb between augite and carbonate liquid at 55 kbar and 1200°C. *Trans. Am. Geophys. Union.* V21C-11 (Fall Meeting)

Wood B. J. and Blundy J. D. (1997) A predictive model for rare earth element partitioning between clinopyroxene and anhydrous silicate melt. *Contrib. Mineral. Petrol.* **129,** 166–181.

Yaxley G. M., Crawford A. J. and Green D. H. (1991) Evidence for carbonatite metasomatism in spinel peridotite xenoliths from western Victoria, Australia. *Earth Planet. Sci. Lett.* **107,** 305–317.

Yaxley G. M., Green D. H. and Kamenetsky V. (1998) Carbonatite metasomatism in the southeastern Australian lithosphere. *J. Petrol.* **39,** 1917–1930.